



AMERICAN UNIVERSITY OF BEIRUT

SOLAR-ASSISTED DESICCANT DEHUMIDIFICATION  
SYSTEM TO IMPROVE PERFORMANCE OF EVAPORATIVELY  
COOLED WINDOW IN HOT AND HUMID CLIMATES

by  
NABIL AHMAD BLEIBEL

A thesis  
submitted in partial fulfillment of the requirements  
for the degree of Master of Engineering  
to the Department of Mechanical Engineering  
of the Maroun Semaan Faculty of Engineering and Architecture  
at the American University of Beirut

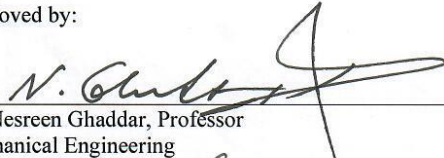
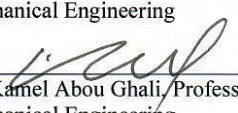

Beirut, Lebanon  
June 2020

AMERICAN UNIVERSITY OF BEIRUT

SOLAR-ASSISTED DESICCANT DEHUMIDIFICATION SYSTEM  
TO IMPROVE PERFORMANCE OF EVAPORATIVELY COOLED  
WINDOW IN HOT AND HUMID CLIMATES

by  
NABIL AHMAD BLEIBEL

Approved by:

 _____	[Signature]
Dr. Nesreen Ghaddar, Professor Mechanical Engineering	Advisor
 _____	[Signature]
Dr. Kamel Abou Ghali, Professor Mechanical Engineering	Co-Advisor
 _____	[Signature]
Dr. Joseph Zeaiter, Professor Baha and Walid Bassatne Department Chemical Engineering and Advanced Energy	Member of Committee

Date of thesis defense: June 16, 2020

AMERICAN UNIVERSITY OF BEIRUT

THESIS, DISSERTATION, PROJECT RELEASE FORM

Student Name:

Bleibel                                      Nabil                                      Ahmad  
Last    First    Middle

Master's Thesis                       Master's Project                       Doctoral Dissertation

I authorize the American University of Beirut to: (a) reproduce hard or electronic copies of my thesis, dissertation, or project; (b) include such copies in the archives and digital repositories of the University; and (c) make freely available such copies to third parties for research or educational purposes.

I authorize the American University of Beirut, to: (a) reproduce hard or electronic copies of it; (b) include such copies in the archives and digital repositories of the University; and (c) make freely available such copies to third parties for research or educational purposes after:

- One ---- year from the date of submission of my thesis, dissertation, or project.
- Two ---- years from the date of submission of my thesis, dissertation, or project.
- Three ---- years from the date of submission of my thesis, dissertation, or project.



Signature

23/6/2020

Date

## ACKNOWLEDGMENTS

The authors would like to acknowledge the financial support of the American University of Beirut – University Research Board – Grant award no. 103780.

# AN ABSTRACT OF THE THESIS OF

Nabil Ahmad Bleibel for Master of Engineering  
Major: Applied Energy

Title: Solar-assisted desiccant dehumidification system to improve performance of evaporatively cooled window in hot and -humid climates

This study examines the performance of an integrated evaporatively-cooled window (ECW) with a desiccant dehumidification system (DDS) combined with a photovoltaic/thermal (PV/t) system. The hybrid system (ECW-DDS) is applied on a glazed building surface to reduce its temperature and the associated space-cooling load. The system performance is studied during the summer months with hot and humid conditions in which the benefits of passive cooling systems are generally restricted. Mathematical models for each system component/process were integrated to predict the system effectiveness for a case study of a typical office space located in Jeddah, Kingdom of Saudi Arabia. The integrated system effectiveness was compared to two cases where the system was not installed for a clear double glass window and where only the ECW system is employed without the dehumidification of ambient air. The hybrid system (ECW-DDS) proved to reduce the inner window temperature by 5 °C, 7 °C, 4 °C, and 5 °C for June, July, August, and September, respectively resulting in an 11% decrease of the total cooling load over the summer months. In addition, the ECW-DDS system performed much better than the ECW system when humid conditions prevailed in September. For instance, the air leaving the evaporative cooler on a typical day of September recorded a temperature reduction of 14% in the case of the ECW-DDS system compared to 1% only in the case of the ECW system.

# CONTENTS

ACKNOWLEDGEMENTS.....	v
ABSTRACT.....	vi
LIST OF ABBREVIATIONS .....	ix
LIST OF ILLUSTRATIONS.....	xi
LIST OF TABLES.....	xiii
Chapter	
1. INTRODUCTION.....	1
2. SYSTEM DESCRIPTION .....	6
2.1. The dehumidification and evaporative cooling systems .....	8
2.2. The regeneration and power supply system .....	9
3. MATHEMATICAL MODELING.....	11
4. NUMERICAL METHODOLOGY .....	19
5. CASE STUDY .....	22
5.1. Selection of the system components .....	24
5.2. Number of PV/t panels in parallel .....	25
6. RESULTS AND DISCUSSION .....	28
6.1. Optimal number of parallel PV/t panels .....	29

6.1.1. Constraint regarding the minimum regeneration temperature .....	30
6.1.2. Constraint regarding the hourly-average temperature difference between the air flowing adjacent to the glazing section and the ambient air .....	31
6.2. The effect of regeneration temperature on humidity ratio for Case I	33
6.3. Comparison of the temperature of the air leaving the evaporative cooler (Case I and Case II) .....	37
6.4. Analysis of the glazing temperature.....	40
6.5. Analysis of the space cooling load.....	45
6.6. Psychrometric chart of the air states for each summer month.....	47
6.7. Water consumption in evaporative cooler.....	48
<b>7. ECONOMIC IMPLICATIONS AND BENEFITS OF THE PROPOSED SYSTEM.....</b>	<b>51</b>
<b>8. LIMITATIONS AND APPLICABILITY.....</b>	<b>53</b>
<b>9. CONCLUSION.....</b>	<b>54</b>
<b>BIBLIOGRAPHY .....</b>	<b>56</b>



## NOMENCLATURE

$A$	area ( $\text{m}^2$ )
$c_p$	specific heat ( $\text{J/kg}\cdot\text{K}$ )
$C$	cost (\$)
$DDS$	desiccant dehumidification system
$e_s$	sensible efficiency
$E$	energy (KJ)
$ECW$	evaporatively cooled window
$H$	enthalpy (KJ)
$h_c$	heat convection coefficient ( $\text{W/m}\cdot\text{K}$ )
$h_{fg}$	latent heat of vaporization of the water ( $\text{J/kg}$ )
$h_m$	mass convection coefficient (m/s)
$h_r$	radiative heat transfer coefficient ( $\text{W/m}^2\cdot\text{K}$ )
$Hr$	Hour
$I$	solar radiation ( $\text{W/m}^2$ )
$\dot{m}$	mass flow rate (kg/s)
$n$	year number
$N$	number of panels
$NPV$	net present value (\$)
$PV$	Photovoltaic
$PV/t$	photovoltaic/thermal
$Q$	load (W)
$Q_{internal}$	internal heat gain load (W)
$RH$	relative humidity (%)
$T$	temperature ( $^{\circ}\text{C}$ )
$T$	thickness (m)
$U$	velocity (m/s)
$V$	volumetric flow rate (cfm)
$W$	width (m)
$W$	humidity ratio (kg of $\text{H}_2\text{O}$ /kg of dry air)
$w^*$	humidity ratio of saturated air (kg of $\text{H}_2\text{O}$ /kg of dry air)
$X$	horizontal position (m)

*Y* vertical position (m)

### **Greek Symbols**

*P* density (kg/m<sup>3</sup>)

### **Subscripts**

*A* air  
*air-glazing* air flowing adjacent to glazing section  
*air-evap* air in the evaporative cooler  
*amb* ambient  
*B* black plate  
*Cr* inside the office room  
*des-out* desiccant wheel outlet  
*elec* electrical  
*g* glass cover  
*Gap* Gap  
*ga* daily water consumption  
*gsky* the glass cover and the sky  
*i* Inner  
*in* Inlet  
*Irr* irradiance  
*m* Mass  
*min* minimum  
*o* Out  
*og* outer glass  
*r* radiation  
*ag* the absorber/substrate and glass cover  
*reg* regeneration  
*room* office room  
*s* substrate  
*sens-out* sensible wheel outlet  
*Sky* Sky  
*Su* supply  
*Wall* Wall  
*wat* Water  
*Win* window  
*1* upper channel of PV/t  
*2* lower channel

## ILLUSTRATIONS

Figure	Page
1. The 3D schematic of the proposed system .....	7
2. Schematic of (a) the proposed system and (b) air property changes on the psychrometric chart .....	8
3. Schematic of (a) the desiccant wheel and (b) the PV/t used in the dehumidification phase.....	12
4. Exporative cooler model.....	17
5. Glazing Section model.....	18
6. Flow chart of the proposed numerical model .....	20
7. PV/t panels configuration.....	25
8. Flow chart to find the optimal number of panels.....	27
9. Hourly distribution of the regeneration temperature vs the ambient temperature and the reduction in humidity ratio for a typical June day in Jeddah.....	36
10. Hourly distribution of the regeneration temperature vs the ambient temperature and the reduction in humidity ratio for a typical July day in Jeddah.....	36
11. Hourly distribution of the regeneration temperature vs the ambient temperature and the reduction in humidity ratio for a typical August day in Jeddah.....	37
12. Hourly distribution of the regeneration temperature vs the ambient temperature and the reduction in humidity ratio for a typical September day in Jeddah.....	37
13. Hourly distribution of the inner window temperature for different cases in (a) June (b) July (c) August and (d) September.....	41
14. Hourly distribution of cooling load for different cases in (a) June (b) July (c) August and (d) September.....	46

15. Psychrometric charts showing the air thermodynamic states for (a) June, (b) July, (c) August, and (d) September at hour 16:00.....	48
16. Hourly distribution of water consumption in July.....	50
17. Payback period for ECW-DDS proposed system (Case I) compared to conventional (Case III) .....	52

## TABLES

Table	Page
13. Ambient conditions for typical days in each summer month [42] .....	23
14. Space envelope used in the case study [18].....	23
15. Reported relative error of measurement of each model.....	29
16. Comparison of the hourly average temperature of the air leaving the evaporative cooler and the minimum regeneration temperature for different number of PV/t panels during summer months.....	30
17. Comparison of the air temperature leaving the evaporative cooler between Case I and Case II for all summer months.....	38

# CHAPTER 1

## INTRODUCTION

The building sector accounts for nearly one-third of global greenhouse gas emissions and for more than 40% of global energy demand [1, 2]. Due to the negative impact of increased energy consumption on global warming, architects are compelled to design more energy efficient buildings [3, 4]. Air conditioning loads have increased rapidly during last few decades primarily because of improvements in life quality, rapid urbanization, and availability of reliable and multi-sized air conditioning units [5, 6]. About 32% of the building sector's electricity consumption is attributed to air-conditioning systems worldwide [7] but in hot regions such as the Gulf, this percentage could be much higher. During the summer in Abu Dhabi, United Arab Emirates, 80% of the electricity is used to meet the air-cooling demand [8]. Moreover, many studies have reported that glazed surfaces are among the main elements that contribute to the high air conditioning load in buildings in hot and humid climates [9, 10]. As a result, modeling air conditioning systems is necessary for studying and regulating the energy consumption in buildings [11].

In recent years, designing large glazing areas has become an essential feature of modern architecture especially in office spaces. In Dubai, United Arab Emirates, 80% of buildings use fully glazed facades signaling a growing trend [3, 12]. This shift towards glazed envelope is a result of their contribution to adding esthetic features to the building facades, increasing the natural lighting, and ensuring a suitable

environment for employees in the offices that can increase their productivity [13]. Although glazed surfaces are essential in modern designs, they represent the weakest thermal component of the building envelope that can be easily affected by outdoor conditions. Direct solar radiation is transmitted through windows to the building environment, where part of it is absorbed by the space internal surfaces and then radiated to the indoor environment while the other part is absorbed by the glazed surfaces that increases their temperature [13]. Consequently, glazed surfaces are among the main parameters that contribute to the increase of cooling loads in buildings in hot climates [14-16].

Therefore, extensive research has been done on how to reduce the space load due to glazed surfaces with many solutions developed. These studies considered the orientation of the glazing surfaces in the buildings with results showing a required 25% savings in the cooling load [17]. However, this solution can only be implemented in the design and construction of new buildings since it may not be feasible for existing buildings [18]. Other solutions included the use of absorptive material like vanadium dioxide thermo-chromic glass, which could reduce the cooling load by 40% but this method proved relatively expensive [18]. Passive techniques have been also the focus of many researchers to reduce the space load [19]. Among them is the design of single and dual airflow windows to reduce the window surface temperature [20, 21]. These windows allow natural airflow through their cavities due to the presence of temperature difference between the inner and outer surfaces. However, this method requires

additional ventilation load of fresh air to the space in order to compensate for the air exhausted through the window.

Each of the above-mentioned solutions has some limitations in its performance or cost, which brings the need to develop others that use a relatively cheap glazing system that is feasible to implement in existing buildings with good performance without compromising daylight. In this regard, Al Touma et al. [18] proposed a system that combined the principles of passive evaporative cooling and solar chimneys to reduce window surface temperature. Their system was applied to an office space located in the city of Riyadh in the Kingdom of Saudi Arabia (KSA) and was found to reduce the total cooling load by up to 19.8% in spaces having window-to-wall ratios of 40% when clear double pane windows were used. Moreover, the system was able to reduce the sensation of thermal discomfort due to radiation asymmetry with respect to an occupant seated one meter away from the window. However, when the proposed system was applied in the KSA city, Jeddah, energy savings decreased to 13.1%. This proves that the use of the proposed system was limited to dry weather conditions, which restricted its benefits in locations suffering from humid weather conditions such as Jeddah. Therefore, it is of interest to improve the proposed system of Al Touma et al. [18] by extending its applicability to humid weather conditions. This improvement can be achieved by integrating a dehumidification technique that allows the humidity of the ambient air to decrease before reaching the evaporative cooler of the window system.



Various dehumidification techniques are available. In mechanical systems, condensation dehumidification is commonly used. Nevertheless, reheat is needed to warm up the supply air temperature in the case when the cooling source temperature is lower than the dew point of the processed air, resulting in a large cold–heat offset loss [22]. Recently, solid desiccant wheels have received much attention [23, 24], where these wheels have been used for air humidity treatment, dehumidification and enthalpy treatment [25, 26]. Rotary desiccant wheels are effective approaches to air dehumidification that can avoid the cold–heat offset loss and be regenerated with low-grade heat sources [27, 28]. Solid desiccant technology integrated with a solar source of energy is very appealing because it uses a renewable source of energy in the dehumidification process [17, 29, 30]. The importance of such a system is in its ability to remove high amount of moisture from air at low regeneration temperatures that can be easily attained from a solar source. [24, 31].

In the current study, a solid desiccant dehumidification system (DDS) is designed to be incorporated with the evaporative cooled window (ECW) system to dehumidify ambient air before entering the evaporative cooler. Lowering the humidity of air entering the system allows it to be more effectively cooled in the evaporative cooler. To ensure the continuous operation of the desiccant wheel, a regeneration heat source is required. Therefore, a photovoltaic/thermal (PV/t) panel is used to regenerate air and simultaneously supply electric energy to satisfy the electrical demand of the wheels and the fans [32]. Hence, the aim is to investigate the effectiveness of the ECW

when integrated with a desiccant dehumidification system regenerated by a PV/t system in hot and humid climates. Validated mathematical models of various system components are integrated to simulate the performance of the entire system. The integrated model is then used in a simulated case study to assess the window performance over the summer months of the hot and humid climate of Jeddah and will compare performance with and without the window dehumidification system.

The proposed new passive evaporative cooling window system would overcome the issues associated with the hot and humid climate, which in general poses a challenge on implementing effectively any evaporative cooling solution. Hence, a sustainable passive evaporative cooling system design is applied based on incorporating different technologies (DDS and PV/t) to enhance the effectiveness of the ECW system in a typical hot and humid climate.

## CHAPTER 2

### SYSTEM DESCRIPTION

The main objective of the proposed DDS-ECW system is to reduce the temperature of an office space's glazing surface in hot and humid climate conditions like in Jeddah, KSA. Jeddah is selected due to its diverse summer climate that varies between hot and dry (June and July), humid (August), and warm and high humidity (September) [33]. This allows for testing of the proposed system's feasibility in a variety of summer conditions.

To overcome high humidity reducing the effectiveness of evaporative cooling, solid rotary wheels are incorporated with the ECW system of Al Touma et al. [18]. The desiccant (Silica gel) wheel is used to decrease the humidity of the fresh air stream, which is followed by the sensible counter flow wheel consisting of a circular honeycomb matrix. The effect of improving window performance by adding a dehumidification process during hot and humid summer months is investigated and the associated reduction in the cooling load of the proposed system is compared with the load when the system is operated without the dehumidification system.

As shown in **Fig. 1**, the proposed DDS-ECW system is comprised of the following main components: i) the photovoltaic thermal panel (PV/t); ii) the desiccant and the sensible wheels of the DDS system; iii) the evaporative cooler; iv) the glazing section of the ECW. The integrated system is applied to a case study of a typical office space located in Jeddah, KSA.

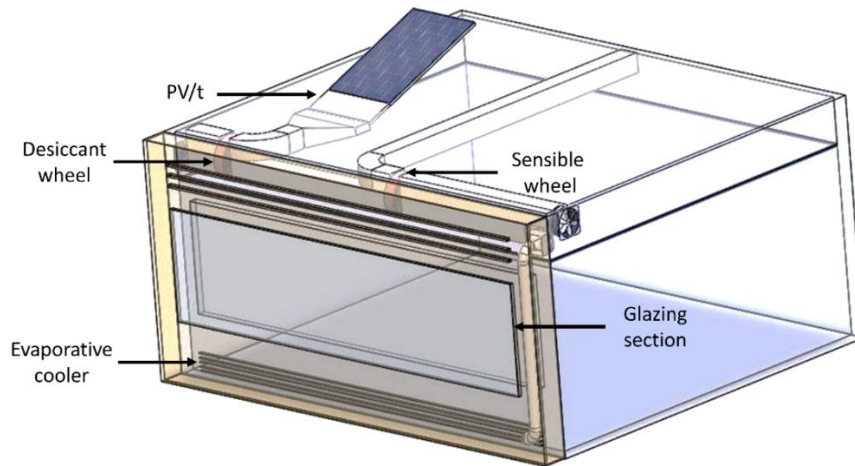


**Fig. 1:** The 3D schematic of the proposed system

**Fig. 2** shows (a) the airflow circulation through the integrated system and (b) the associated thermal processes of the air on the psychrometric chart. The circulations of the supply and the exhaust air are attained through two ducting systems, one supplying ambient air and the other supplying the regenerating air of the desiccant wheel. Thus, the integrated system can be divided into two main subsystems: (I) the dehumidification and window evaporative cooling systems and (II) the regeneration system. Both systems are described in this section.

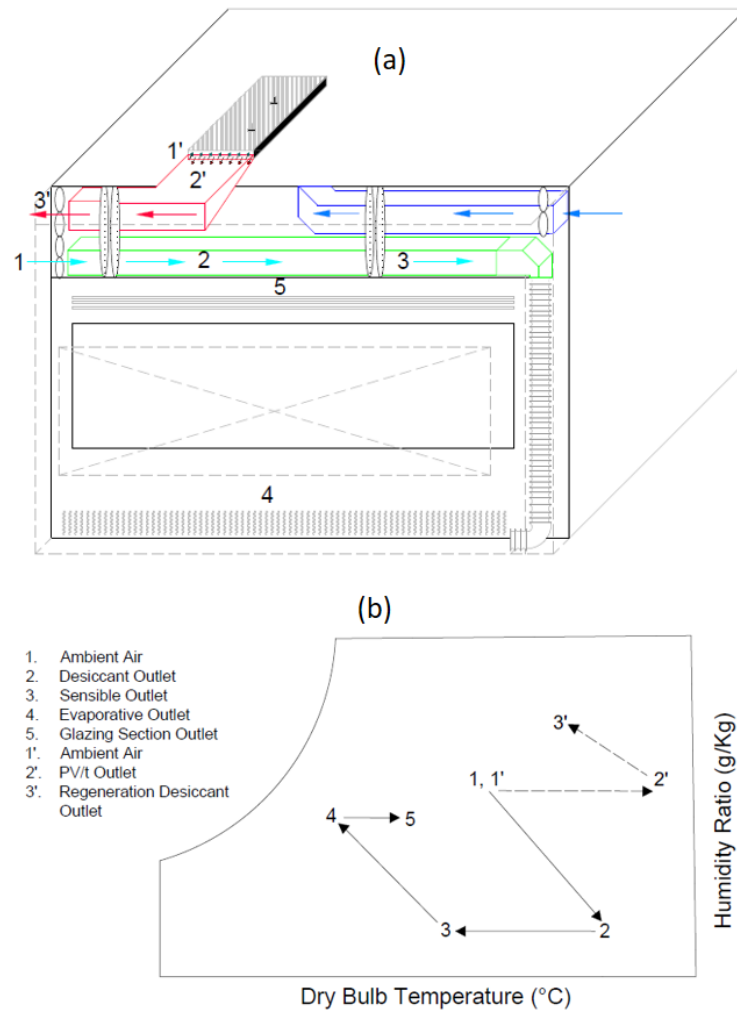


**Fig. 2:** Schematic of (a) the proposed system and (b) air property changes on the psychrometric chart

## 2.1 The dehumidification and evaporative cooling systems

Using an inlet supply fan, ambient air enters the desiccant wheel at state 1 where it is dehumidified before it reaches the sensible wheel at state 2 (**Fig. 2 (a)**). The dehumidification process removes the humidity from the air before reaching the

evaporative cooler to enhance its cooling efficiency [29]. As the air temperature increases after dehumidification (state 2), a sensible wheel is used to exchange the heat at state 2 with the ambient air. The relatively dry cool air then leaves the sensible wheel at state 3 and passes through the evaporative cooler. The evaporative cooler consists of water absorbing sheets at the channel walls below the window, as well as, a water reservoir and a pump to ensure the continuous flow of water [18]. The evaporative cooler cools the incoming air by evaporating the water at the wet channel walls leading to a decrease of the air temperature to leave the evaporative cooler at state 4.

Afterwards, the evaporatively cooled air at state 4 passes through the glazing section located above the evaporative cooler as shown in **Fig. 2 (a)**. The temperature of the air increases along the window gap until it leaves the system to the environment at state 5. If the glazing is exposed to solar radiation, natural convection aids the forced convection increasing the upward flow of air. The psychrometric process of the proposed system shows the states of air from state 1 to state 5 (see **Fig. 2 (b)**).

## **2.2 The regeneration and power supply system**

The photovoltaic/thermal panel (PV/t) simultaneously produces electricity and heat to effectively utilize the solar energy and achieve higher PV electrical efficiency while making use of the removed heat for regeneration purposes [34]. Therefore, the PV/t mounted at the roof of the building converts the solar radiation into electric energy

to drive one desiccant and one sensible wheel, one water pump, and three fans. The air fans allow (i) the flow of the ambient air through the system, and (ii) the continuous supply of hot air that is used to regenerate the desiccant wheel, (iii) the minimization of the air leakage inside the rotary wheels which can seriously degrade their performance [35]. As shown in **Fig. 2(b)**, the ambient air enters the PV/t at state 1' which is the ambient state and leaves at 2' after being passively heated by solar radiation. The heated air is then used in the desiccant wheel for regeneration purposes and exits the system completely at state 3'.

## CHAPTER 3 MATHEMATICAL MODELING

To study the performance of the proposed DDS-ECW system, the cooling load of the glazed space must be determined and compared to a reference case. However, the calculation of the cooling load necessitates the estimation of the temperature of the air layer adjacent to the glazing section. The air layer temperature is related to the properties of air flowing through the whole system from state 1 to state 4 (**Fig. 2 (b)**). Therefore, it is essential to solve the mass and heat balance equations of the air streams in each phase: i) dehumidification using desiccant wheel and PV/t, ii) sensible heat exchange using sensible wheel, latent heat exchange using evaporative cooler, and iii) heat convection through the glazing section.

*Phase 1: dehumidification using desiccant wheel (state 1 to 2) and PV/t (state 1' to 2'):*

The dehumidification phase is produced using the desiccant wheel regenerated by PV/t panel. The schematics of the desiccant wheel and air-cooled PV/t panel are shown in **Fig. 3**. The desiccant wheel is a constant enthalpy device that exchanges latent energy for sensible energy, leading to dehumidification and heating of the process air stream simultaneously. As shown in **Fig. 3(a)**, the desiccant wheel used in this study is a counter-flow wheel to increase the efficiency of the regeneration process; in one passage, the hot air regenerates the desiccant wheel and is then exhausted to the outside, while in the other passage the air is dehumidified before being supplied to the sensible



wheel. The air required for the regeneration process is heated by the PV/t panels. The PV/t has the advantage of reducing the PV/t panels' operating temperature, which increases the electrical efficiency [34]. The PV/t panel is shown in **Fig. 3 (b)** where ambient air (state 1') enters the upper channel and leaves at a relatively high temperature (regeneration temperature) from the lower channel.

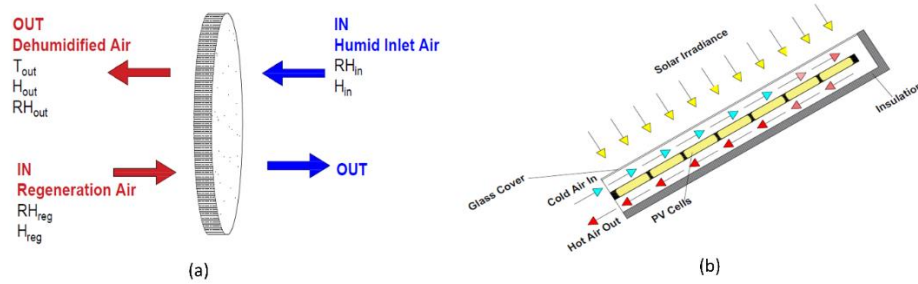


**Fig. 3:** Schematic of (a) the desiccant wheel and (b) the PV/t used in the dehumidification phase

The model developed and validated by Makarem et al. [34] was adopted for the modeling of the dehumidification phase achieved by the desiccant wheel and the PV/t panel. Their model was based on a 1-D steady state heat transfer analysis of the PV/t panel by assuming that the temperature varied only along the length of the PV/T panel and the superstrate and the absorber (PV cells) had the same temperature. Based on the aforementioned assumptions, the energy balances were developed for each layer shown in **Fig. 3(b)**; the upper glass, the airflow in the upper and lower channels, and the superstrate/absorber layers.

The upper glass gains solar irradiance and radiative heat flux from the absorber of the glass cover while losing heat by radiation to the sky and by convection to both the

ambient air and the air flowing in the upper channel. Thus, the energy balance [34] of the upper glass is determined by

$$I_{irr} + h_{rag} (T_s - T_g) = h_{rgsky} (T_g - T_{sky}) + h_{cgw} (T_g - T_{amb}) + h_{cga1} (T_g - T_{a1}) \quad (1)$$

where  $I_{irr}$  is the of solar irradiance hitting the surface of the PV/t,  $h_{rag}$ , and  $h_{rgsky}$  are the radiative heat transfer coefficients between the absorber/substrate and glass cover, and between the glass cover and the sky, respectively.  $h_{cgw}$  and  $h_{cga1}$  are the convective heat transfer coefficients between the glass cover and outdoor air, and between the glass cover and air in upper channel, respectively.  $T_s$ ,  $T_g$ ,  $T_{sky}$ ,  $T_{amb}$ , and  $T_{a1}$  are the temperatures of substrate, glass cover, sky, outdoor air, and air in upper channel, respectively. Similarly, the model developed all energy balances of the air flowing in the upper channel, the superstrate layer that is gaining power from PV cells, the air flowing in the lower channel, as well as, the back-plate layer [34].

The ambient air entering the PV/t panel (state 1') was heated while flowing in the upper and lower channel and left the PV/t panel (state 2') which was used in the regeneration of the desiccant wheel. In order to model the dehumidification process in the desiccant wheel, the model of Beccali et al. is adopted [36]. To predict the outlet temperature and humidity of the air stream passing through the rotary desiccant wheel, the adopted model was derived from the interpolation of experimental data obtained from the industry to come up with correlations that can accurately evaluate the performance of rotary desiccant wheels in terms of different parameters [36]. The

correlations were used by other researchers in the literature showing good results [37, 38, 39] and are given as follows:

$$H_{des-out} = 0.1312H_{reg} + 0.8688H_{in} \quad (2)$$

$$RH_{des-out} = 0.9428RH_{reg} + 0.0572RH_{in} \quad (3)$$

where  $H_{des-out}$ ,  $H_{in}$ ,  $H_{reg}$  are the enthalpies of the air leaving, entering, and regenerating the desiccant wheel, respectively. Likewise,  $RH_{des-out}$ ,  $RH_{in}$ ,  $RH_{reg}$  are the relative humidity of the air leaving, entering, and regenerating the desiccant wheel, respectively.

Furthermore, their model established an empirical correlation for the outlet air temperature that was used as an inlet to sensible wheel model in the next phase [36]:

$$\frac{RH_{des-out}e^{0.053T_{des-out}-1.7976}}{18671} = \frac{H_{des-out}-1.006T_{des-out}}{2501-1.805 T_{des-out}} \quad (4)$$

As mentioned earlier, the adopted model is based on correlations developed from experimental data. Therefore, these equations (2-4) are only valid for the following ranges: 20 °C to 34 °C for the inlet air temperatures; 40 °C to 80 °C for the regeneration temperatures; 8 to 15 g/kg for the inlet air humidity ratio; and 10 to 16 g/kg for the humidity ratio of the regeneration air [36].

*Phase 2: sensible heat exchange by means of sensible wheel (state 2 to 3):*

In this phase, the air stream leaving the desiccant wheel at state 2 is being introduced to a sensible wheel in order to drop its temperature. From the equation of the

sensible effectiveness  $e_s$ , the temperature of air leaving the sensible wheel is estimated by the following equation:

$$T_{sens-out} = \frac{e_s \times V_{min} (T_{amb} - T_{des-out})}{V_{su}} + T_{des-out} \quad (5)$$

where  $T_{sens-out}$ ,  $T_{des-out}$ , and  $T_{amb}$  are the temperature of air leaving the sensible wheel, the temperature of air leaving the desiccant wheel, and the air ambient temperature, respectively.  $V_{su}$  is the supply air volumetric flow rate and  $V_{min}$  is the minimum between the exhaust and the supply volumetric flow rate (cfm). The sensible effectiveness,  $e_s$ , of the heat recovery wheel was selected at 85% based on the experimental data of Alghamdi et al. [40]. Since Phase 2 is based on the sensible heat exchange, the air stream flowing through the sensible wheel does exchange latent heat as follows:

$$w_{sens-out} = w_{des-out} \quad (6)$$

where  $w_{sens-out}$  and  $w_{des-out}$  are the humidity ratio of air leaving the sensible wheel and the humidity ratio of air leaving the desiccant wheel.

### *Phase 3: Evaporative cooler (state 3 to 4)*

The schematic of the horizontal evaporative cooler is shown in **Fig. 4**. Air enters the horizontal evaporative cooler at  $T_{des-out}$  and  $w_{des-out}$  (state 3). The moving air in the evaporative cooler's channel exchanged mass through convection with the water absorbing sheets installed in the evaporative cooler internal surfaces. The governing equations of this current phase were those developed by Al Touma et al. [18]. In their

model, they assumed a channel width much larger than its gap, which allowed for treating the system as airflow between two parallel plates. Consequently, the mass balance equation of the air in this section is given by

$$\rho_{air-evap} \times u_{air-evap} \times t_{gap} \times \frac{dw_{air-evap}}{dx} = 2 \times \rho_{air-evap} \times h_m (w^* - w_{air-evap}) \quad (7)$$

The left side of equation (7) represents the mass flux of the air passing through the evaporative cooler whereas the right side represents the moisture gain as the air evaporates the water circulating at the sides of the evaporative cooler, where  $w^*$  is the humidity ratio of saturated air at water temperature.

The energy balance equation of the air passing through the evaporative cooler is governed by the following equation [18]:

$$\rho_{air-evap} \times C_{p_{air-evap}} \times u_{air-evap} \times t_{gap} \times \frac{dT_{air-evap}}{dx} = 2 \times h_c (T_{wat} - T_{air-evap}) + 2 \times \rho_{air-evap} \times h_m \times h_{fg} (w_{air-evap} - w^*) \quad (8)$$

where  $h_c$  and  $h_m$  are the heat and mass convection transfer coefficient.  $T_{air-evap}$  and  $T_{wat}$  are the temperatures of air in the evaporative cooler channel and the water supplied to the evaporative cooler.  $T_{wat}$  is assumed constant due to the continuous water supply through the pump and  $h_{fg}$  represents the latent heat of water supplied to the evaporative cooler. The left side of equation (8) represents the heat flux of the air whereas the right side represents the heat losses of the air due the latent and sensible convection heat transfer as the air moves through the channel of the

evaporative cooler. Using the heat/mass transfer analogy and assuming a Lewis number of unity, the convection mass transfer coefficient ( $h_m$ ) is given by

$$h_m = \frac{h_c}{\rho_a \times C p_a} \quad (9)$$

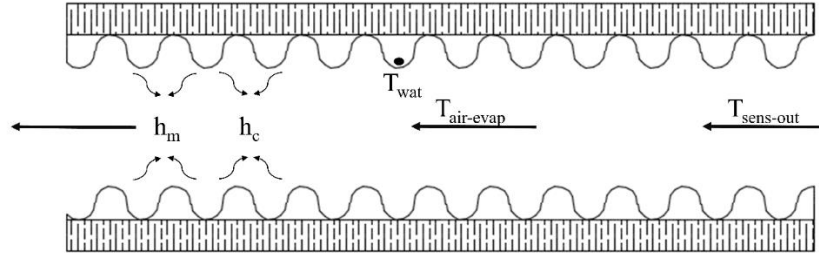


Fig. 4: Evaporative Cooler Model

*Phase 4: heat convection through the glazing section (state 4 to 5)*

As shown in **Fig. 5**, the glazing section is divided into three main layers: the outer glass, the air gap, and the window layers. Thus, as air flows in the glazing section it exchanges heat with the inner layer of the outer glass and the outer layer of the window by means of forced convection. Therefore, the energy balance of the air layer is given by

$$\rho_{air-glazing} \times C p_{air-glazing} \times u_{air-glazing} \times t_{gap} \times \frac{dT_{air-glazing}}{dy} = h_c (T_{og,i} - T_{air-glazing}) + h_c (T_{win,o} - T_{air-glazing}) \quad (10)$$

where  $T_{og,i}$ ,  $T_{win,o}$ , and  $T_{air-glazing}$  are the temperatures of the outer layer of the outer glass, the temperature of the outer surface of the window, and the temperature of air circulating.  $h_c$  is the convection heat transfer coefficient due to the air passing

between the window and the outer glass mainly driven by the inlet air fan considered running at a constant speed [41].

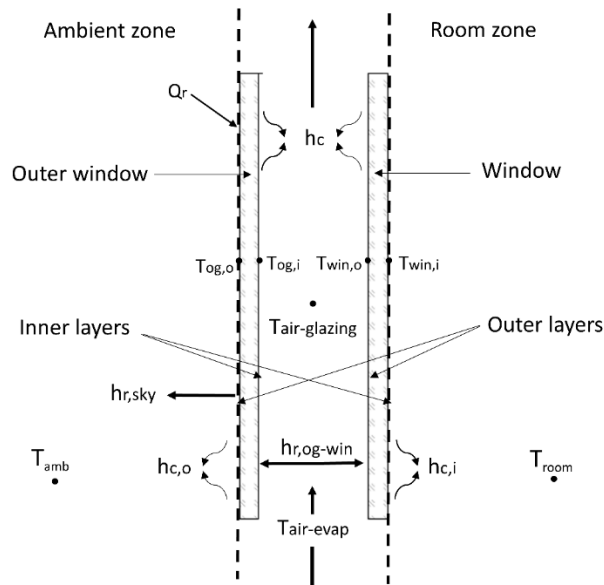


**Fig. 5:** Glazing Section Model

Energy balance equations were also carried out for each of the remaining layers to solve for the outer glass, and window outer ( $T_{og,o}$ ,  $T_{win,o}$ ) and inner ( $T_{og,i}$ ,  $T_{win,i}$ ) surface temperatures as detailed in [18] and are not to be repeated here. These energy balances consider radiation absorbed and transmitted by surfaces, radiation exchange between surfaces, conduction through the outer glass and window, as well as, the convection of outdoor, induced, and indoor air with different surfaces.

## CHAPTER 4

### NUMERICAL METHODOLOGY

The objective of this section is to present the numerical methodology used to solve the temperatures and humidity as applicable at the different exit states of each system in the integrated models in an office equipped with the proposed system in hot and humid ambient conditions. The flow chart of the numerical methodology for each hour is presented in **Fig. 6**.

For each hour  $i$ , all the weather conditions (temperature, humidity, irradiance), as well as, the dimensions of PV/t and the electrical power needs were first entered into the PV/t model where the energy balances of the PV/t layers were discretized along the longitudinal direction. Once all the energy balances were solved for each node, the properties of the leaving air at the last node of the lower channel were considered as the regeneration properties at this hour and were used as input values to the desiccant model as shown in the flow chart of **Fig. 6**. Therefore, the hourly regeneration properties were related to the PV-t dimensions, power, and the outdoor conditions of the office space. The desiccant model used the regeneration properties as inputs to predict the air conditions leaving the desiccant wheel. Likewise, the sensible wheel model used the desiccant wheel model output parameters and estimated the properties of the air leaving. The evaporative cooler needed the water temperature, the air flow rate, as well as, the evaporative cooler characteristics as input to calculate the properties of air leaving the evaporative cooler. The evaporative cooler model was based on discretizing the air layer



into several nodes and on solving the energy balance for each node. The outlet conditions of the air leaving the evaporative cooler were used as input for the glazing section.

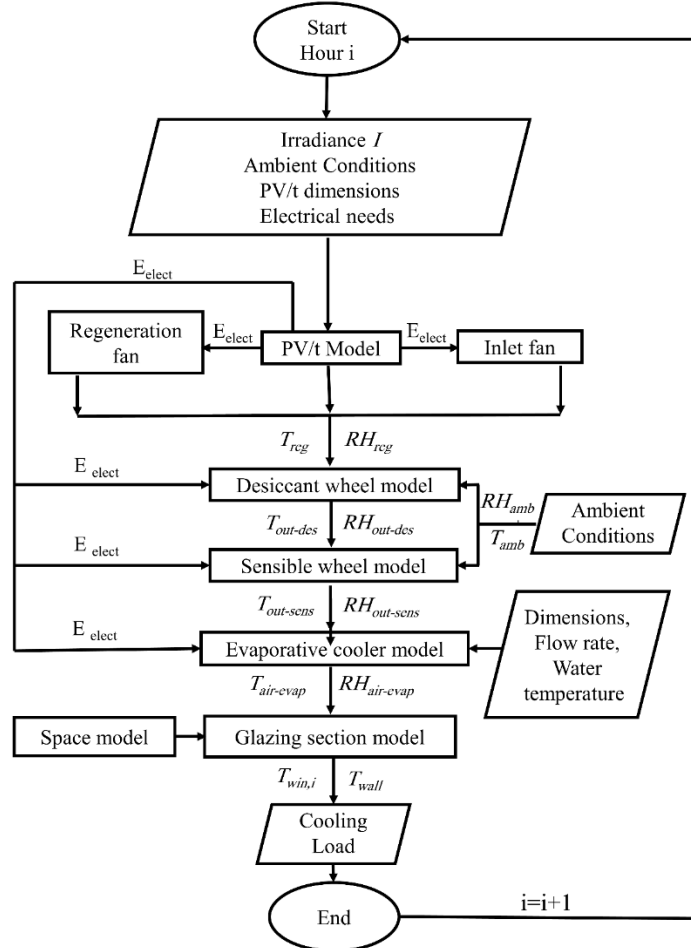


Fig. 6: Flow chart of the proposed numerical model

Moreover, the space dimensions and the heat load of each component in the room were required as input to the glazing section for the calculation of the window and the wall temperatures of the room. The calculated temperatures of the inner, outer glass,

window, and walls were assigned initial arbitrary temperatures while the mass and heat balance equations were discretized into algebraic equations. The temperatures of the room walls and the window were then used to calculate the space model cooling load at each hour  $i$  using the following equation:

$$Q_{hvac} = \sum Q_{wall} + h_{cr} \times A_{win}(T_{win,i} - T_{room}) + Q_{internal} \quad (11)$$

where  $h_{cr}$  is the convection heat transfer coefficient between the air inside the room and the inner window surface,  $A_{win}$  is the surface area of the glazing,  $T_{room}$  is the room air temperature,  $\sum Q_{wall}$  is also the sum of the convective heat transfer rate between the air inside the room and the walls, and  $Q_{internal}$  is the internal heat gain within the space.

## CHAPTER 5

### CASE STUDY

The proposed DDS-ECW system is applied to a case study of a typical office space ( $6\text{ m} \times 5\text{ m} \times 3\text{ m}$ ) in the hot and humid climate of Jeddah. The office is maintained at a room temperature of  $22\text{ }^{\circ}\text{C}$  with a constant occupancy of two people from 8:00 until 18:00. The DDS-ECW performance and effect on office thermal load were considered during the summer months from June to September using a typical representative day for each month. The weather data of the four representative days of summer months are presented in **Table 1**. The office space had its South and West walls exposed to the outdoor conditions while the other walls were partitioned with conditioned spaces. The West facade had a window with dimensions  $5.5\text{ m} \times 1.4\text{ m}$  installed at its center. The characteristics of the space envelope used in this case study are summarized in **Table 2**. The evaporative cooler was installed horizontally to benefit from a larger contact area between the flowing air and the evaporative cooler channel. This is achieved by an inlet air fan with the ability to move the air regardless of the orientation of the air channel. Therefore, the evaporative cooler was designed with dimensions of  $5.5\text{ m}$  in length and a width of  $0.7\text{ m}$ . The temperature of the water supplied to the evaporative cooler was set as the night temperature of the studied day.

**Table 1:** Ambient conditions for typical days in each summer month [42].

Time	June			July			August			September		
	$T_{amb}$ (°C)	$RH_{amb}$ (%)	$I$ (W/m <sup>2</sup> )	$T_{amb}$ (°C)	$RH_{amb}$ (%)	$I$ (W/m <sup>2</sup> )	$T_{amb}$ (°C)	$RH_{amb}$ (%)	$I$ (W/m <sup>2</sup> )	$T_{amb}$ (°C)	$RH_{amb}$ (%)	$I$ (W/m <sup>2</sup> )
8:00	30	55	110	31	55	104.63	33	63	99.35	35	82	93.00
9:00	32	46	147	32	52	143.08	35	49	139.62	36	81	132.00
10:00	34	44	175	34	41	172.51	37	50	170.04	35	81	160.30
11:00	36	37	194	35	32	192.71	38	50	190.65	36	79	180.52
12:00	35	39	309	35	34	328.43	40	45	317.52	35	79	301.32
13:00	34	44	345	35	34	330.84	40	45	346.27	35	73	329.10
14:00	34	46	548	36	34	540.45	39	50	562.47	34	75	550.00
15:00	34	46	705	37	32	705.57	38	46	729.26	33	77	718.65
16:00	34	49	789	38	30	796.52	35	53	812.54	33	77	800.50
17:00	34	46	757	36	30	770.48	34	67	756.78	33	77	750.50
18:00	35	39	515	36	32	527.17	34	67	405.67	33	77	395.30

**Table 2:** Space envelope used in the case study [18]

Parameter	Material
Internal Walls	2 cm gypsum board + 28 cm air gap + 2 cm gypsum board
External Walls	2 cm plaster + 20 cm concrete + 2 cm plaster
Floor and Ceiling	15 cm light concrete
Window	Clear double glazing
Outer Glass	Clear single glazing

## 5.1 Selection of the system components

The selected desiccant wheel model was RVB-700 with a diameter of 70 cm, which fit perfectly inside the duct [43]. The wheel's electrical consumption was 93 W. The associated sensible wheel was a HRW-19-250 EcoFresh heat recovery wheel with an electrical consumption of 82 W [44]. The ducts are made of insulated galvanized steel [45, 46]. The insulation is applied to control heat loss through duct walls. The fiberglass insulation is resistant to mold growth and fiber erosion in accordance with industry standards and will avoid the distribution of airborne mold or glass fibers [47].

The moderate water requirements of the evaporative cooling channel are met with a small pump whose electrical consumption is minimal. For instance, a positive displacement pump that suited such an application and which met the water flow rate requirements (0.4 L/hr) typically had a nominal power of less than 90 W.

The regenerated air flowing from PV/t system to the desiccant wheel and the ambient air supplied to the desiccant and sensible wheel was supplied by using three inlet air fans of minimal electrical consumption not exceeding 15 W [34]. Typical mono-crystalline silicon  $1.65 \times 1 \text{ m}^2$  PV modules with a nominal power rating of 350 W<sub>p</sub> each at 21.49 % efficiency were used in this study [48]; however, the number of PV/t panels needs to be determined using the PV/t model as detailed in the next subsection.

## 5.2 Number of PV/t panels in parallel

A number of PV/t panels is used to regenerate the desiccant wheel and to provide the electrical power needed to operate the wheels, fans, and pump. These PV/t panels are connected in parallel as shown in **Fig. 7** with a common header where the air mass flow rate is divided into  $n$  panels and then collected to regenerate the desiccant wheel. It is important to highlight that finding the optimal number of parallel PV/t panels needed to regenerate the desiccant wheel and to provide the power to operate the wheels, fans, and pump is necessary. Since electric power needs are minimal, the thermal energy delivery at desired regeneration temperature is the controlling parameter for the number of parallel panels to meet this requirement.

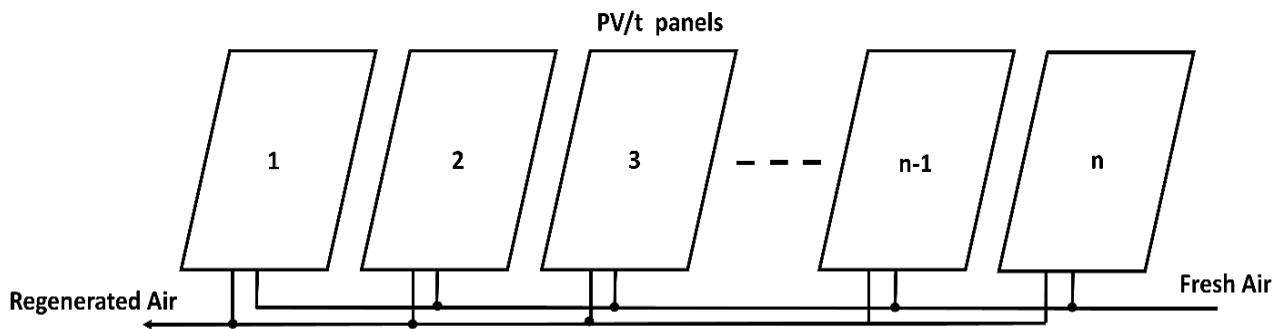


Fig. 7: PV/t panels configuration

To avoid oversizing the system, the optimal number is considered as the minimum number of parallel PV/t panels that can deliver sufficient thermal energy to regenerate the desiccant wheel for all the summer months. This minimum number of parallel PV/t panels must ensure sufficient dehumidification of the ambient air such that that the temperature of the air leaving the evaporative cooler and flowing adjacent to the

glazing section is significantly less than the ambient temperature. This is achieved by simulating the integrated model of the DDS-ECW for different number of panels until reaching the desired outputs. The regeneration temperature varies hourly since it depends on the hourly solar radiation and ambient temperature. Thus, when the system is sized by means of PV/t panels' number, the design should always be effective even when solar radiation is low during the early hours. Hence, the minimum regeneration temperature is analyzed for its ability to regenerate the desiccant wheel at all operational hours.

The methodology of choosing the number of parallel PV/t panels was based on incrementing  $n$  by 1 starting from 1 until that the hourly average temperature of the air flowing adjacent to the glazing section was less than the ambient temperature by at least 5°C for all summer months. The second constraint was based on Beccali et al. [36], stating that the minimum regeneration temperature must exceed 40°C to be able to regenerate the desiccant wheel. When these two constraints were met, the number of parallel PV/t panels was no longer incremented, and the optimal value of  $n$  was reached as shown in the flow chart of **Fig. 8**.

The total mass flow rate of air flowing through parallel PV/t panels that was used in the simulations was around 0.01 kg/s which was the typical air mass flow rate reported in the literature [49, 50].

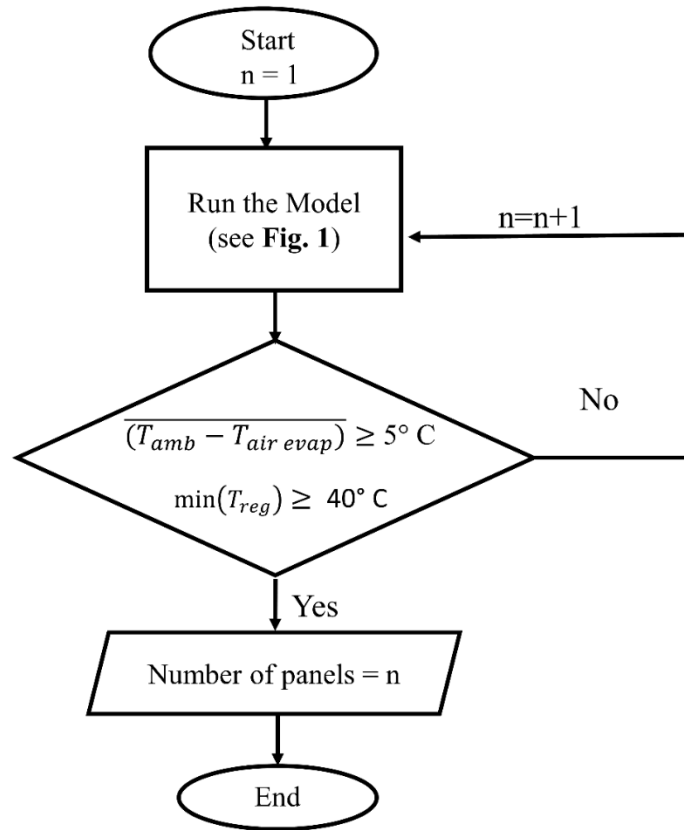


**Fig. 8:** Flow chart to find the optimal number of panels



## CHAPTER 6

### RESULTS AND DISCUSSION

The proposed system was evaluated based on the simulations of the developed mathematical model during typical days of the summer months from June to September and for a typical office space in Jeddah, KSA. In addition, the effectiveness of the proposed system was assessed by comparing the cooling load of the office space in three cases:

- i) **Case I:** The current proposed integrated DDS-ECW system where the ambient humid air is undergoing a dehumidification before reaching the evaporative cooler.
- ii) **Case II:** The ECW system without dehumidification of the ambient air entering the evaporative cooler [18].
- iii) **Case III:** Conventional clear double pane window.

The accuracy of the obtained results depends on the accuracy of the PV/t model, desiccant model, evaporative cooler model, and heat convection in the glazing section model. These models are experimentally validated models with a small relative error compared to the experimental findings shown in **Table 3**. Moreover, the overall operation has a small error of measurement and high accuracy, which makes the obtained model results reliable.

**Table 3:** Reported relative error of measurement of each model

Model	Error in temperature (°C)	Error in humidity ratio (g/kg)
PV/t model [51]	$\pm 2.78$	-
Desiccant model [36]	$\pm 1.85$	$\pm 1.00$
Evaporative cooler [18]	$\pm 1.07$	$\pm 1.08$
Glazing model [18]	$\pm 1.16$	-

The analysis started by determining the optimal number of PV/t panels followed by consideration of effectiveness of the DDS, the air cooling through the evaporative cooler, and finally the impact of cooled air on the glazing section and space cooling load.

### **6.1 Optimal number of parallel PV/t panels**

As described in section 5.2, the optimal number of parallel PV/t panels was found by repeating the mathematical model simulations for a number of panels starting from  $n = 1$  and incremented by 1 until the constraints shown in the flow chart of **Fig. 8** were met. The simulation results for different number of PV/t panels over the summer months are summarized in **Table 4**.

**Table 4:** Comparison of the hourly average temperature of the air leaving the evaporative cooler and the minimum regeneration temperature for different number of PV/t panels during summer months

Number of PV/t	June ( $\overline{T_{amb}}=33.8$ °C)		July ( $\overline{T_{amb}}=35$ °C)		August ( $\overline{T_{amb}}=36.6$ °C)		September ( $\overline{T_{amb}}=34.3$ °C)	
	Min ( $T_{reg}$ ) (°C)	$\overline{T_{air-evap}}$ (°C)	Min ( $T_{reg}$ ) (°C)	$\overline{T_{air-evap}}$ (°C)	Min ( $T_{reg}$ ) (°C)	$\overline{T_{air-evap}}$ (°C)	Min ( $T_{reg}$ ) (°C)	$\overline{T_{air-evap}}$ (°C)
<i>n=1</i>	37.20	27.125	37.03	26.23	39.97	30.23	40.77	31.32
<i>n=2</i>	38.74	26.67	38.51	25.86	41.41	29.68	42.12	30.63
<i>n=3</i>	39.57	26.40	39.33	25.67	42.20	29.36	42.86	30.39
<i>n=4</i>	40.13	26.34	39.86	25.52	42.72	29.17	43.35	29.75
<i>n=5</i>	40.53	26.26	40.26	25.53	43.10	29.04	43.71	29.3

### 6.1.1 Constraint regarding the minimum regeneration temperature

The lowest regeneration temperature for all summer months increased as the number of PV/t panels increased (see **Table 4**). Evidently, when the number of PV/t panels increased, the air mass flow rate passing in each PV/t panel decreased leading to an increase in the difference of temperature between the air flowing and the panel surface. Thus, the regeneration temperature increased.

It is important to point out that observing the difference in regeneration temperature between the summer months is necessary. September, for example, reached

the desired  $T_{reg}$  using one PV/t panel while August needed two panels. July and June needed four and five panels, respectively. The optimal panel number was related to the hour in the day at which the minimum regeneration temperature occurred for each month. All the summer months had minimum regeneration temperature at 8:00 in the morning because of the relatively low solar radiation. However, even during this time September had the highest ambient temperature of 35 °C followed by August (33 °C), July (31°C), and lastly June (30 °C) (see **Table 1**). September was only 5 °C away from the minimum regeneration temperature of 40 °C, which proves why one panel was sufficient. Thus, to meet the minimum regeneration temperature constraint over all the summer months, five PV/t panels were selected which corresponded to the month of June.

### ***6.1.2 Constraint regarding the hourly-average temperature difference between the air flowing adjacent to the glazing section and the ambient air***

When the regeneration temperature increased, the humidity ratio of air decreased thus increasing its ability to absorb water vapor and releasing heat in the evaporative cooler. When using one PV/t panel, the reductions of the hourly average temperature of air leaving the evaporative cooler were 7.24 °C, 9.24 °C, 7.07 °C, and 3.99 °C for June, July, August, and September, respectively. This reduction in air temperature was maximum in July because it had the highest hourly average solar radiation (419 W/m<sup>2</sup>) followed by June (417 W/m<sup>2</sup>), and then August (411 W/m<sup>2</sup>) while

September had the lowest value of 401 W/m<sup>2</sup>. In addition, September was considered the most humid month in Jeddah based on weather and climate [33]. These two factors resulted in having the lowest reduction in the temperature of air leaving the evaporative cooler in September. Therefore, one panel was insufficient to regenerate the desiccant wheel in September and more panels were needed to increase this reduction in temperature. Furthermore, when the number of panels reached five, the temperature of the air leaving the evaporative cooler was reduced by 7.55 °C, 9.48 °C, 7.5 °C, and 5 °C for June, July, August, and September, respectively. Therefore, the two constraints (i)  $\min(T_{reg}) \geq 40 \text{ °C}$  and (ii)  $(T_{amb} - T_{air\ evap}) \geq 5 \text{ °C}$  were satisfied when the number of PV/t panels reached five.

Five PV/t panels were more than enough to meet the electrical requirement of the proposed system components. The total electrical consumption of the system components (one desiccant wheel, one sensible wheel, three fans, and one water pump) in a working day of 10 hours (from 8:00 hr. to 18:00 hr.), was estimated to be at 3.1 kWh. The electrical energy afforded by one PV/t panel module was around 1.4 kWh on a typical day in July in Jeddah, thus three PV/t panels were sufficient to meet the electrical requirements of the system components. Furthermore, the electrical power of the remaining PV/t panels could be used for office electrical needs [52]. The PV/t panels are used to afford both electricity and thermal energy, however, the electrical consumption of the system components is minimal, while the thermal energy needed is

significant. Thus, the regeneration temperature (the thermal energy) is the tradeoff for the proposed system.

## **6.2 The effect of regeneration temperature on humidity ratio for Case I**

5 PV/t panels oriented towards the west as described in the case study were used to regenerate the desiccant wheel to increase its ability to absorb water vapor and therefore release more heat in the evaporative cooler. **Fig. 9-12** show the hourly distribution of the regeneration temperature compared to the ambient temperature, as well as, the humidity ratio of air leaving the desiccant wheel for the summer months in Jeddah.

The regeneration temperature is related to the ambient air temperature and the outdoor solar radiation. It is clear from **Fig. 9-12** that the regeneration temperature profile was always increasing and reached its peak between 15:00 hr. and 17:00 hr. exceeding 75 °C for all summer months [52]. This is because the solar radiation always increased from the morning (at 8:00 hr.) to reach a maximum between 15:00hr. and 17:00 hr. exceeding 700 W/m<sup>2</sup> for all summer months (see **Table 1**). On the other hand, the humidity ratio of the air leaving the desiccant wheel showed an opposite trend to the regeneration temperature over all months. It was observed that the humidity ratio decreased from the morning to reach its minimum between 15:00 hr. and 17:00 hr. when the regeneration temperature was reaching its maximum (see **Fig. 9-12**). This was justified by the effect of regeneration in decreasing the humidity ratio of the air flowing

through the desiccant wheel even though the regeneration temperature did not exceed 45 °C for all months during the early morning hours (e.g. 8:00 and 9:00 hr).

The highest regeneration temperature was reached during a regular day in July at 16:00 hr; 88 °C when the solar radiation was around 800 W/m<sup>2</sup> and the ambient air temperature was 38 °C. Although August showed higher solar radiation than July (812 W/m<sup>2</sup>) at the same time, the ambient temperature was 3 °C less. Therefore, July presented the highest regeneration temperature, which led to a maximum decrease in humidity ratio at this time between the air leaving the desiccant wheel and the ambient air, at 54%.

Moreover, the thermal energy absorbed from the five PV/t panels over the summer months were as follows: 3 kWh/day, 2.9 kWh/day, 2.22 kWh/day, and 2.8 kWh/day for the typical days of June, July, August and September, respectively. This thermal energy was related to the difference between the ambient temperature and the regeneration temperature (see **Fig. 9-12**).

September is the most humid summer month (see **Fig. 12**) where the ambient air humidity varied between 0.024 at hour 15:00 (kg of H<sub>2</sub>O/kg of dry air) and 0.031 (kg of H<sub>2</sub>O/kg of dry air) at hour 9:00 while solar radiation varied between 93 W/m<sup>2</sup> at 8:00 hr. to 800 W/m<sup>2</sup> at 16:00 hr. Consequently, the regeneration temperature varied between 43 °C at 8:00 hr. and 85 °C at 16:00 hr. Since the regeneration temperature was relatively low at 8:00 hr., the humidity ratio was only reduced by 1%; thus, the system was ineffective at this time. Nevertheless, the humidity ratio was further reduced as time

increased. At noon when the regeneration temperature reached 55 °C, the humidity ratio decreased by 11 %. The maximum reduction in humidity ratio exceeded 37% for September at 16:00 hr. and this was justified by the relatively high regeneration temperature related to the high solar radiation at this time (800 W/m<sup>2</sup>). This major reduction in humidity ratio affects the temperature of the air leaving the evaporative cooler as will be discussed in the next sub-section.



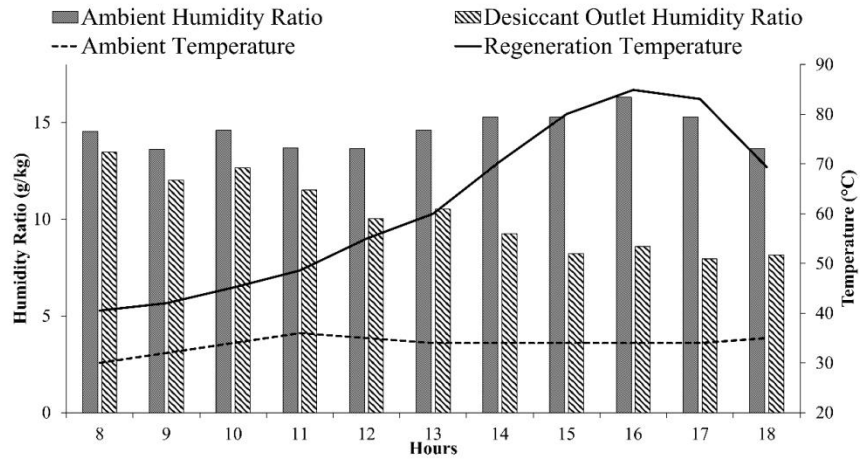


Fig. 9: Hourly distribution of the regeneration temperature vs. the ambient temperature and the ambient vs. desiccant outlet humidity ratio for a typical June day in Jeddah

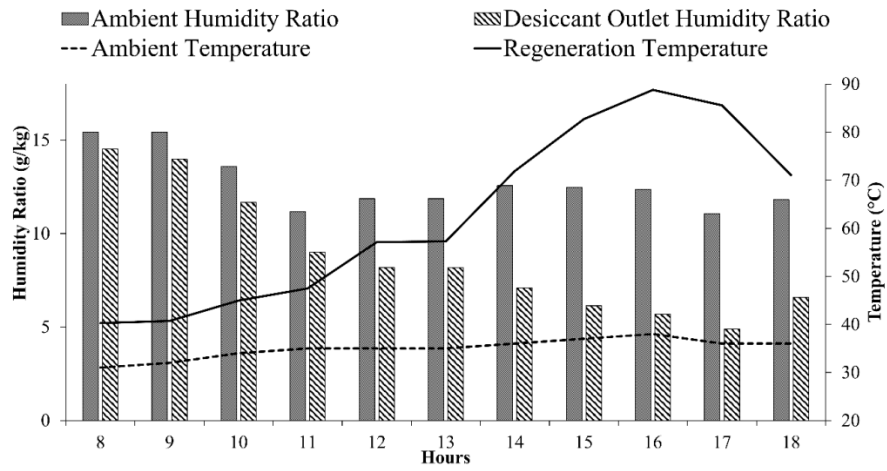


Fig. 10: Hourly distribution of the regeneration temperature vs. the ambient temperature and the ambient vs. desiccant outlet humidity ratio for a typical July day in Jeddah

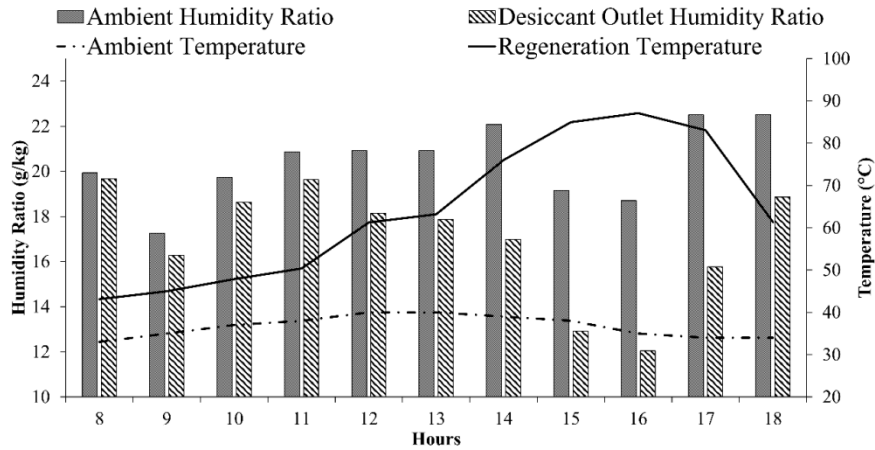


Fig. 11: Hourly distribution of the regeneration temperature vs. the ambient temperature and the ambient vs. desiccant outlet humidity ratio for a typical August day in Jeddah.

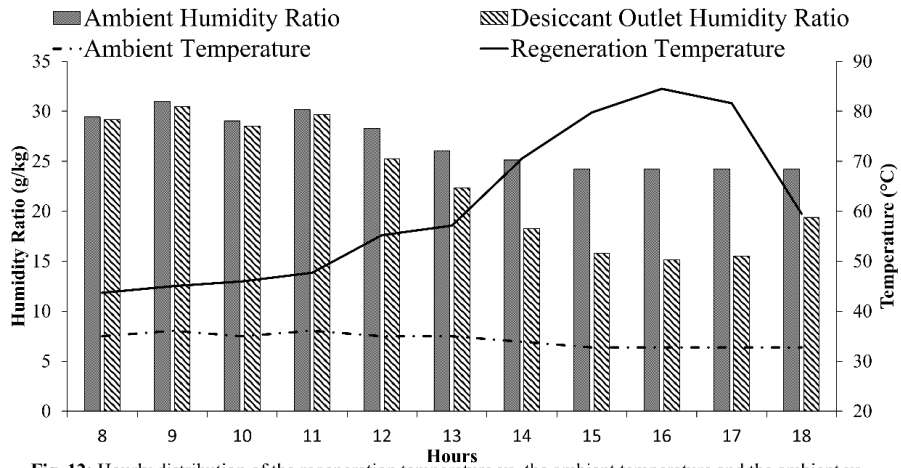


Fig. 12: Hourly distribution of the regeneration temperature vs. the ambient temperature and the ambient vs. desiccant outlet humidity ratio for a typical September in Jeddah.

### 6.3 Comparison of the temperature of the air leaving the evaporative cooler (Case I and Case II)

The temperature of the air leaving the evaporative cooler is compared between Case I (DDS-ECW system) where the ambient humid air undergoes a dehumidification

before reaching the evaporative cooler and Case II (ECW system) where the ambient air is not dehumidified before entering the evaporative cooler. The results of the four summer months are summarized in **Table 5**. All the summer months achieved a reduction in the temperature of the air leaving the evaporative cooler compared to the ambient conditions. However, Case I and Case II have different effects in the temperature reduction of the air leaving the evaporative cooler. All the summer months had higher temperature reduction in Case I when dehumidification was incorporated compared to Case II when no dehumidification took place.

**Table 5:** Comparison of the air temperature leaving the evaporative cooler between Case I and Case II for all summer months

Time (hr)	June			July			August			September		
	T <sub>amb</sub> (°C)	T air-evap (°C)		T <sub>amb</sub> (°C)	T air-evap (°C)		T <sub>amb</sub> (°C)	T air-evap (°C)		T <sub>amb</sub> (°C)	T air-evap (°C)	
		Case I	Case II		Case I	Case II		Case I	Case II		Case I	Case II
8:00	30.00	24.66	25.94	31.00	25.51	25.60	33.00	27.41	27.45	35.00	33.6	34.9
9:00	32.00	25.68	26.38	32.00	26.10	26.61	35.00	27.52	27.75	36.11	33.71	36.01
10:00	34.00	28.09	29.05	34.00	26.50	27.45	37.00	31.1	31.34	35.00	31.4	35
11:00	36.00	29.32	30.51	35.00	25.71	26.89	38.00	32.73	33.09	36.11	31.3	36.01
12:00	35.00	27.31	29.45	35.00	25.14	27.35	40.00	33.29	35.11	35.00	30.63	34.91
13:00	34.00	26.67	29.10	35.00	25.13	27.38	40.00	33.2	35.14	35.00	29.11	34.9
14:00	34.00	25.55	29.51	36.00	25.42	28.82	39.00	30.9	34.84	33.89	27.76	33.86
15:00	34.00	25.12	29.42	37.00	25.77	29.75	38.00	27.15	31.97	32.78	25.74	32.16
16:00	34.00	25.43	30.09	38.00	26.50	30.67	35.00	23.58	28.71	32.78	25.8	32.15

17:00	34.00	24.93	29.45	36.00	23.95	29.84	34.00	25.05	30.1	32.78	25.72	32.17
18:00	35.00	26.10	29.39	36.00	25.07	28.31	34.00	27.56	30.1	32.78	27.85	32.15

As shown in Case II, the average reduction in the temperature of the air leaving the evaporative cooler compared to ambient was 14%, 20%, 14%, and 1% for June, July, August, and September, respectively. July presented the largest reduction of the air temperature while September presented the lowest reduction of the air temperature, which could be neglected. This was expected since air was not dehumidified before reaching the evaporative cooler in Case II. The relatively high humidity ratio of September led to less latent heat exchange of outdoor air with the water sheets in the evaporative cooler resulting in relatively higher air temperature. On the other hand, since July was the driest summer month (see **Table 1**) the system in Case II was able to reduce the air temperature because of the high capability of air to absorb latent heat in the evaporative cooler.

When the DDS-ECW system of Case I was adopted, the average reduction in the temperature of the air leaving the evaporative cooler for September increased from 1% to 14%. This is related to the reduced humidity ratio (see **Fig. 12**). In addition, the average reduction in the temperature of the air leaving the evaporative cooler for July increased from 20% to 27%. This modest increase was related to the dry weather conditions of Jeddah in July compared to the other summer months.

It is of interest to focus on the performance of the system in Case I and II for September, the most humid summer month. In the early hours, the temperatures of the air leaving the evaporative cooler were very close to the ambient conditions for both Case I and II. This was due to the high humidity of the air not being dehumidified in the absence of the desiccant wheel in Case II and the insignificant solar radiation in Case I. When the solar radiation became sufficient enough to regenerate the desiccant wheel of Case I, the temperature of the air leaving the evaporative cooler decreased to a minimum of 25.72 °C compared to 32.17 °C in Case II at 17:00 hr. Therefore, in humid conditions like September, the system adopted in this study (Case I) was effective in decreasing the temperature of the air leaving the evaporative cooler to flow over the glazing section unlike Case II where dehumidification did not take place.

#### **6.4 Analysis of the glazing temperature**

The novelty of the DDS-ECW system has been argued in its ability to overcome the harsh and humid conditions for effective window cooling in which Case II's system developed in the literature [18] did not significantly decrease the glazing temperature. Hence, a comparison is performed of the hourly distributions of the window inner surface temperature between three cases; Case I (DDS-ECW), Case II (ECW), and Case III (conventional glazing) when applied to the office space in Jeddah for the summer months as shown in **Fig. 13**.

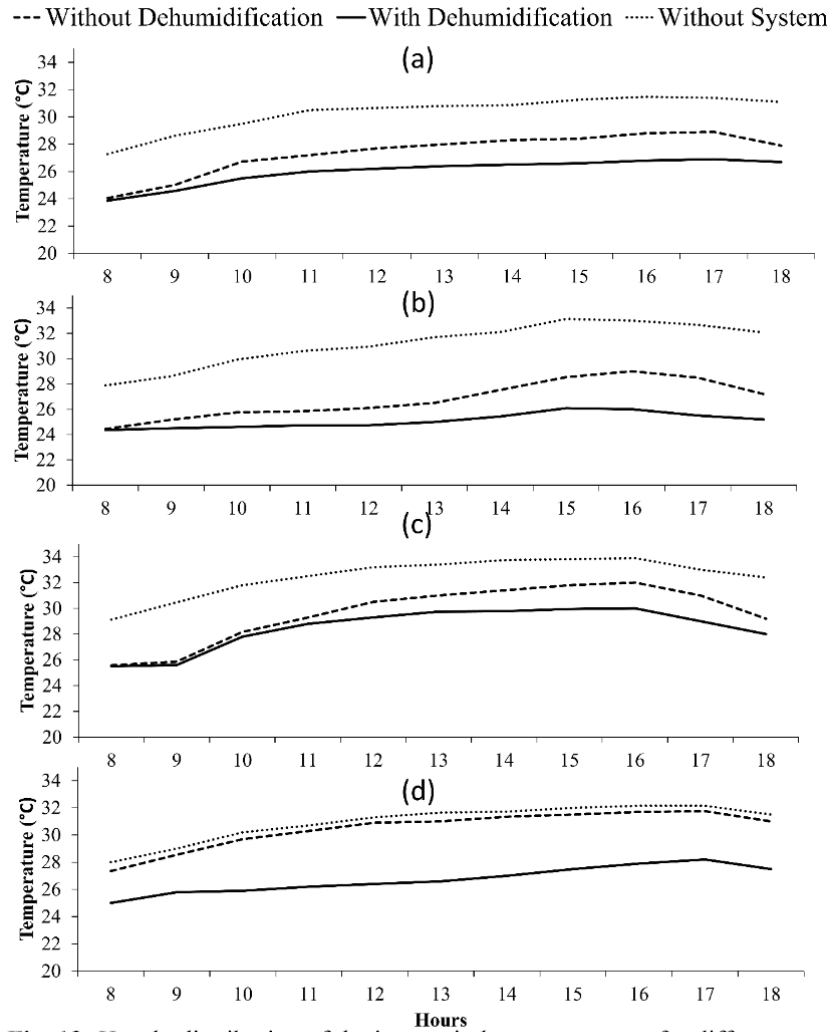


**Fig. 13:** Hourly distribution of the inner window temperature for different cases in (a) June (b) July (c) August and (d) September.

The inner window temperature is related to different factors: (i) inner convection with the air in the room (set at 22 °C) (ii) solar radiation (iii) radiation from the outer layer of the inner window ,and most importantly (iv) the convection with the air flowing adjacent to the glazing section. Therefore, the inner window temperature depends on the temperature of air flowing adjacent to the glazing section which in turn

depends on the system adopted. For instance, in Case III the air flowing adjacent to the glazing section is the ambient air while it is the air leaving the evaporative cooler in Case I and II.

**Fig. 13** shows that for all summer months and in all cases, the inner window temperature was increasing until 17:00 hr and then started decreasing. It was clear that the inner window temperature was affected by the ambient temperature and the solar radiation. Although the ambient temperature did not have a daily and large temperature difference in the summer months, the solar radiation had significant daily variation from 8:00 hr. to 17:00 hr., which then decreased after this time interval. Therefore, the profile of the inner window temperature was primarily affected by the solar radiation. When no system was installed (Case III) for all summer months the inner window temperature was relatively high compared to other cases exceeding 31 °C. The glazing section's relatively high temperature increases the sensible space load which will be further explained in the next section. The inner temperature for all summer months reached its maximum at 16:00 hr. in Case III and were 31.4 °C, 33.99 °C, 33.9 °C, and 31.5 °C for June, July, August, and Sptember, respectively.

When the ECW system without dehumidification of the ambient air entering the evaporative cooler (Case II) was adopted, all the summer months presented a reduction in the glazing temperature of about 9%, 14%, 9% for June, July, and August, respectively compared to Case III as shown in **Fig. 13 (a), (b), and (c)**. Only 1% reduction in September occurred (see **Fig. 13(d)**). These findings were consistent with

those of the evaporative cooler temperatures presented in section 6.3. The largest decrease was achieved by July because of the dry characteristics that allowed air to absorb more water vapor, increasing the release of latent heat in the evaporative cooler and thus, increasing the reduction in the inner window temperature. However, the humid condition of September limited the performance of the system adopted in Case II and only 1 % of reduction was recorded.

The DDS-ECW system (Case I) in this study anticipated the effect of the dehumidification phase of the air before reaching the evaporative cooler to increase the latent heat exchange with the water sheets and consequently increased the ability of air to extract heat from the window surface leading to a decrease in inner window temperature. Although the system adopted in Case II led to a reduction of the inner window temperature for June, July, and August further reductions were recorded when dehumidification took place (Case I). This is clearly seen in **Fig. 13 (a-c)** where the reductions in inner window temperature became 14%, 19%, and 12% for June, July and, August respectively. Any further reduction in the air humidity ratio before reaching the evaporative cooler led to an additional improvement of the water vapor exchange with the water sheets of the evaporative cooler and consequently increased the reduction in the air temperature leading to a decrease of the inner window temperature.

Since the reduction of the humidity took place at the desiccant wheel that needed regeneration, the maximum effect of dehumification in increasing the reduction in the inner window temperature took place between 15:00 hr. and 17:00 hr. where the



solar radiation was sufficient enough to regenerate the desiccant wheel. As shown in **Fig. 13 (a-c)**, the large difference in the inner window temperature occurred at this time interval and reached 5 °C, 7 °C and 4 °C for June, July, and August, respectively.

September recorded a reduction of 14% of the inner window temperature in Case I compared to 1% in Case II. When applying the DDS-ECW system (Case I), the inner window temperature decreased by a maximum of 5°C compared to 1.5°C in Case II when the dehumidification system was excluded (see **Fig. 13 (d)**). Nonetheless, this improvement when dehumidification was applied occurred in the time interval of 15:00hr. -17:00 hr where relative humidity was significant but also was solar radiation intensity. Note that the substantial increase of the regeneration temperature at this time interval (see **Fig. 12 (d)**) resulted in a substantial decrease in humidity ratio (up to 40%), as well as, a substantial decrease in the temperature of air leaving the evaporative cooler reaching 6 °C as shown in **Table 5**. Therefore, air was dehumidified at this time interval allowing for a major enhancement of exchange in latent heat and a major decrease in the window air temperature.

Therefore, it is clear that the system adopted in Case I recorded major improvement in decreasing the inner window temperature for the summer months especially for September where the humid conditions limited the ability of the system adopted in Case II to decrease the inner window temperature.

### ***6.5 Analysis of the space cooling load***

The cooling load of the office case study in Jeddah was estimated using equation (11) for all cases. The cooling load is related to the office wall temperatures, the glazing temperature, and other fixed internal loads. As a result, the cooling load should vary between the different cases in a similar manner as the inner window temperature.

**Fig. 14 (a-d)** illustrates the cooling variation during the summer days of June, July, August, and September for the three different cases. When no system was installed (Case III), the total cooling load needed was around 5 kWh/m<sup>2</sup>. When the system was installed without dehumidification (Case II), the total cooling load of the summer months decreased by 7%; however, when the dehumidification phase is integrated (Case I), the total cooling load of the summer months decreased by 11%. For all summer months, the maximum decrease of the space load between the case of non-dehumidification (Case II) and the case with dehumidification (Case I) occurred between 15:00 hr. and 17:00 hr. when the solar radiation was sufficient to dehumidify the air before entering the evaporative cooler. Even when the ambient conditions were not humid, the DDS-ECW system (Case I) still resulted in a reduction of the cooling load which reached 10% compared to 8% in Case II at 16:00 hr. Evidently, this was related to the increased capacity of air to absorb water vapor and remove sensible heat at glazing section resulting in a decrease of the inner window temperature.

September recorded the maximum reduction in the cooling load when Case I and Case II were compared. Note that the cooling load on the typical day of September was only reduced by a maximum of 0.6% in Case II whereas it reached 11% in Case I at 16:00 hr. This shows the importance of applying the system adopted in Case I especially during the time when the space load attained the peak due to the significant solar radiation ( $800 \text{ W/m}^2$ ).

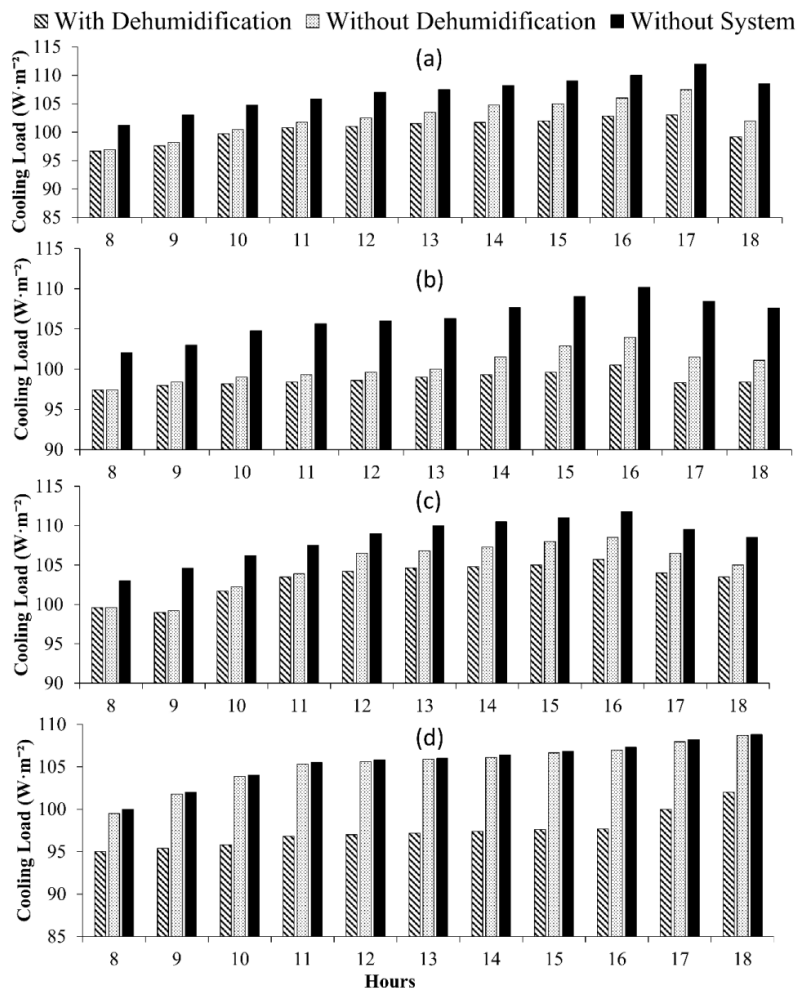


**Fig. 14:** Hourly distribution of cooling load for different cases in (a) June (b) July (c) August and (d) September.

## 6.6 Psychrometric chart of the air states for each summer month

**Fig. 15 (a-d)** shows the psychrometric charts of the air flowing in the system for June, July, August, and September while also showing the thermodynamic air states at hour 16:00. As described in **Fig. (2b)**, the air enters the system at state 1 with a relatively high temperature and a humidity ratio corresponding to the ambient condition for each summer month. After passing through the desiccant wheel, the humidity ratio decreases dramatically (by an average of 40%) while the temperature increases significantly (by an average of 17°C) at state 2. Subsequently, air enters the sensible wheel where the temperature decreases to be close to the ambient temperature conserving the same humidity ratio (state 3). Air then enters the evaporative cooler where its temperature is reduced (by an average of 12°C) because of the latent heat released. However, its humidity ratio is increased (by an average of 60%) to reach state 4 at the inlet of the glazing section. Finally, the forced convection in the air gap between the two glazed surfaces allows the air to exchange heat with the window. Therefore, the air temperature increases (by an average of 2°C) from cooling down the window before leaving to the outside environment at state 5.

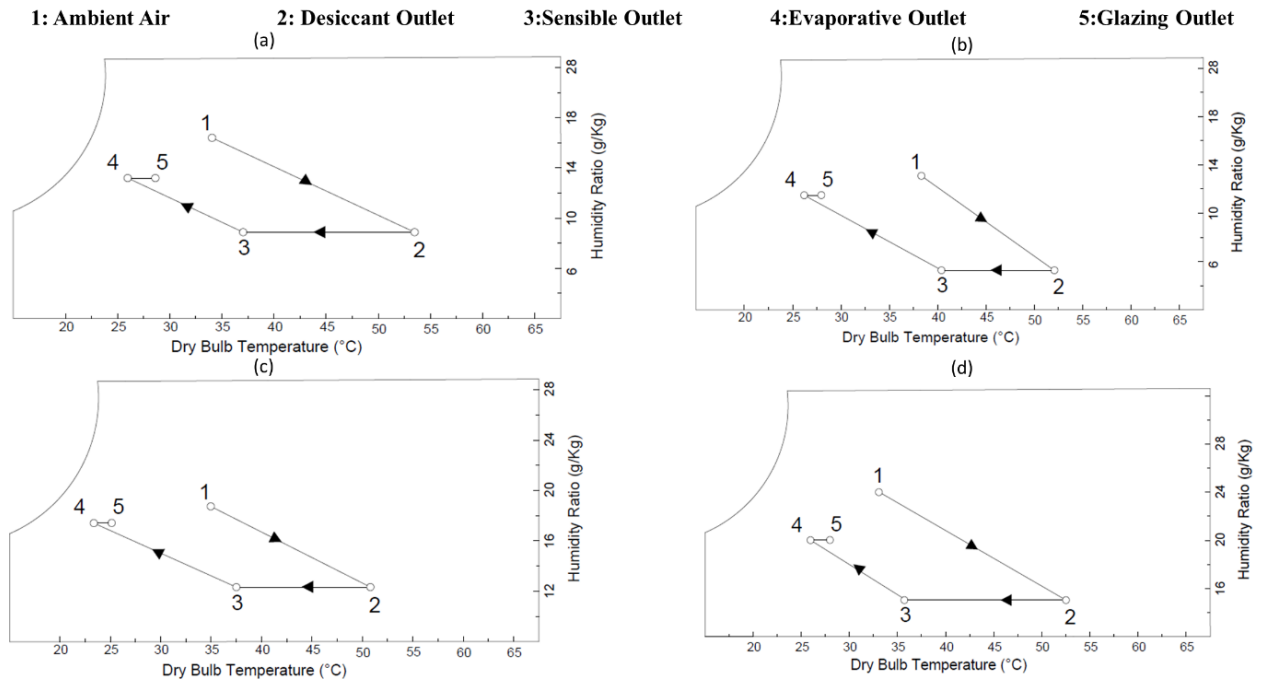


**Fig. 15:** Psychrometric charts showing the air thermodynamic states for (a) June, (b) July, (c) August, (d) and September at hour 16:00

### 6.7 Water consumption in evaporative cooler

When the air enters the evaporative cooler, it absorbs water vapor from the water sheets and release its latent heat leading to a decrease in the air temperature (state 3-4 in **Fig. 15**). In order to ensure the continuous flow of water to the water sheets, a small pump (0.4 l/hr) is used and the excess of water is thrown in a reservoir. Therefore, it is of interest to study the water consumption in the evaporative cooler. Fig. 16 illustrates the hourly water consumption of a typical day of July considered as a typical summer month. As shown in **Fig. 16**, the water consumption ranges from a minimum of

0.09 l/hr in the morning to a maximum of around 0.22 l/hr at hour 17:00. This is because when the air is relatively dry at the inlet of the evaporative cooler, it has a large potential to absorb the moisture from the water sheets [53]. In the morning, for instance at hour 8:00, the relative humidity reaches 49.68% compared to a relative humidity of 11.1% at hour 17:00. Therefore, this maximum moisture absorption at hour 17:00 reflects a maximum water consumption at the same hour.

The daily water consumption of June, July, August and September are 1.5 l/day, 1.8 l/day, 1.5 l/day and 1.2 l/day, respectively during the 10 operating hours. Evidently, the water consumption is minimum in September since this month is the most humid summer month and maximum in July since this month is the driest summer month. This minimal daily amount of water consumption could be due to the condensate drain of the air conditioning systems [54]. The water collected in the reservoir could be treated using chlorine to disinfect it and kill all the germs so that it could be recycled again to the evaporative cooler by means of the pump.

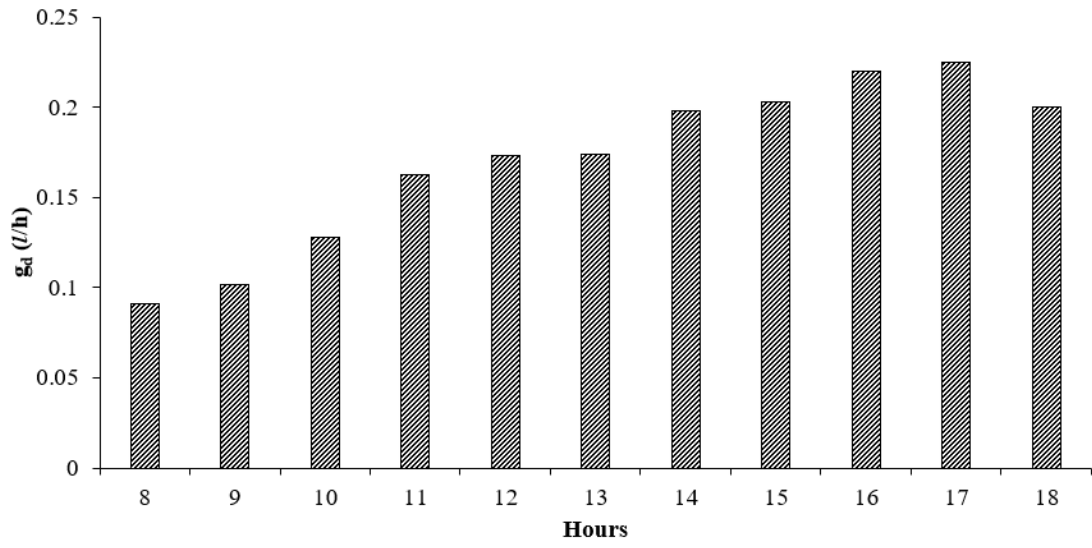


**Fig. 16:** Hourly distribution of water consumption in July

## CHAPTER 7

# ECONOMIC IMPLICATIONS AND BENEFITS OF THE PROPOSED SYSTEM

In this section, an economic feasibility study of the proposed system is developed to assess its pay-back period and savings over the conventional cooling system. For this reason, the life cycle cost NPV (initial + operational) of both systems (Case I and Case III) are calculated [55]. The real discount rate of return is selected as 2% [55] and the period is considered as 20 years.

Since the mechanical cooling system used in the office is common for both cases, its cost is not included in the initial cost. However, since the double glazing used in the conventional system (case III) is replaced by two single-glazing (Case I) (see **Fig. 1**). Therefore, only the difference between these two glazing costs is considered as the initial cost of the conventional system (case III) and it is equal to 825 \$. The initial cost of the proposed system (case I) is 2,000 \$ including the cost of PV/t system [48], the rotary wheels, the water pump, the galvanized ducts and the air fans. The replacement of the water pumps and rotary wheels is assumed to take place once every 15 years to last for the building lifecycle.

To determine the yearly electrical consumption, the cooling load is estimated over the whole year for both cases I and III. The results show a total cooling load of 11 MWh/year for case I compared to 12.4 MWh/year for case III. Moreover, PV/t panels afford electricity of about 3370 kWh/year; all the system components consume around 1.132 kWh/year leading to an excess of 2.238 MWh/year that is used for the office electrical components. Thus, the total electrical consumptions for the conventional system (case III) and the proposed system (case I) are respectively 14.7 and 11 MWh/year.

The average tariff rate of electricity in Jeddah is currently of 48 US cent/kWh [48] with a 2% assumed electricity price growth rate [56]. Therefore, the net present



value or life-cycle cost (NPV) of the conventional system (case III) over 20 years was \$14,660, compared to 12600 \$ for the proposed system (case I) inducing a resultant reduction of 14%. Finally, the payback period of the proposed system was computed by plotting the cumulative net present value for both cases as shown in Fig. 17. It is shown that the pay-back period occurs between 6 and 7 years.

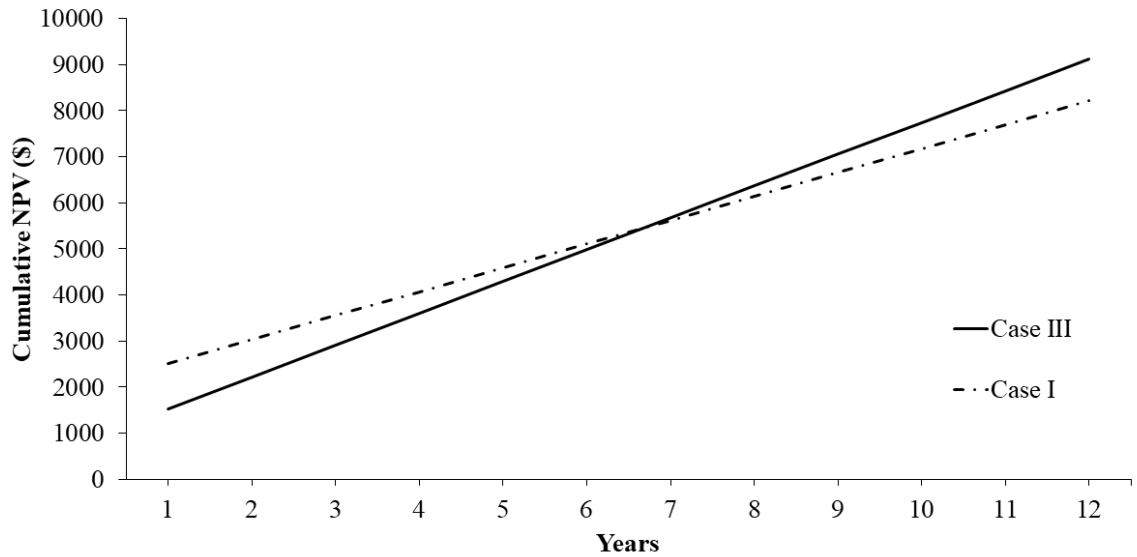


**Fig. 17:** Payback period for ECW-DDS proposed system (Case I) compared to conventional system (Case III)

## CHAPTER 8

### LIMITATIONS AND APPLICABILITY

The proposed study aims to construct a passive window cooling system concurrent with the tendency of new architectural building designs to use facades with large windows. However, there are some limitations like other hybrid systems. The PV/t system is to occupy a roof space not exceeding 20% of the office floor area. Moreover, both the desiccant and the sensible wheel sizes should be selected such that they fit inside the duct system which can be hidden in the false ceiling used for the air distribution system. The remaining duct transporting the air from the sensible wheel to the evaporative cooler could be installed inside the hollow concrete block between the inner and outer glazing.

The applicability of ECW-DDS proposed system design in humid and hot climates has been shown in a case study where the sizing and selection approach as well as their performance prediction models of the various subsystems components were presented for PV/t, the glazing parameters, and the desiccant system parameters under different environmental conditions.. However, any improvement of the design parameters should be investigated while considering life cycle cost analysis.

## CHAPTER 9

### CONCLUSION

A new DDS\_ECW passive technique for reducing the temperatures of glazing surfaces is established and investigated to decrease the cooling load of office spaces especially in hot and humid conditions. The DDS-ECW system is based on dehumidifying the humid air by means of a desiccant wheel regenerated by PV/t panels and conducting the air into an evaporative cooler before flowing adjacent to the glazing surface. A mathematical model integrating the desiccant wheel, PV/t system, sensible wheel, evaporative cooler, and space model, was developed to assess the performance of the system. The proposed system was assessed based on the simulations of the developed mathematical model during the typical days on the summer months from June to September and for a typical office space in Jeddah. The effectiveness of the proposed system was evaluated by comparing the office space cooling load of the proposed DDS-ECW system (Case I) with two other cases: the ECW system without dehumidification of the ambient air entering the evaporative cooler (Case II) and the conventional clear double pane window (Case III).

The results show that the dehumidifying air before reaching the evaporative cooler in the DDS-ECW system brings about a further decrease of the inner window temperature for all the summer months leading to a significant decrease in the cooling load. The key findings of the study are summarized as follows:

1. In humid conditions like in September, the system proposed in this study (Case I) was effective in decreasing the temperature of the air leaving the evaporative cooler to flow over the glazing section (14%) unlike Case II where dehumidification did not take place (1%).
2. The proposed system recorded major improvement in decreasing the inner window temperature during the summer months especially in September where the humid conditions limited the ability of the system adopted in Case II to decrease the inner window temperature. For instance, July recorded a decrease of the inner air temperature by an average of 19% when DDS-ECW system was adopted compared to 14% when no dehumidification occurred (ECW). Moreover, September, which is considered as the most humid summer month, recorded a negligible reduction of the inner window temperature not exceeding 1% when ECW system was adopted compared to 14% when dehumidification was integrated (DDS-ECW).
3. The proposed system recorded a decrease of 11% on the summer cooling load compared to 7% when the system was installed without dehumidification (Case II).
4. A total of 14% reduction in the life cycle cost over 20 years with a 6.5 years payback period.

Therefore, (DDS-ECW) system was found to be very efficient during the summer months of Jeddah especially in September when humidity levels were highest.

## BIBLIOGRAPHY

- [1] S. Kim, P. Zadeh, S. Staub-French, T. Froese, B. Cavka, Assessment of the Impact of Window Size, Position and Orientation on Building Energy Load Using BIM, *Procedia Engineering* 145 (2019) 1424-1431.
- [2] F. Aldawi, A. Date, F. Alam, I. Khan, M. Alghamdi, Energy efficient residential house wall system, *Applied Thermal Engineering* 58 (2013) 400-410.
- [3] M. Towards, Green buildings: Glass as a building element—the use and misuse in the gulf region, *Renewable Energy* 31 (2006) 631-653.
- [4] Kinsara, Adnan A., Moustafa M. Elsayed, and Omar M. Al-Rabghi, Proposed energy-efficient air-conditioning system using liquid desiccant, *Applied Thermal Engineering* 16, 10 (1996) 791-806.
- [5] G. Chaudhary, M. Ali, N.A. Sheikh, S. Khushnood, Integration of solar assisted solid desiccant cooling system with efficient evaporative cooling technique for separate load handling, *Applied Thermal Engineering* 140 (2018) 696-706.
- [6] Gong, Guangcai, Wei Zeng, Liping Wang, Chih Wu, A new heat recovery technique for air-conditioning/heat-pump system, *Applied Thermal Engineering* 28 (2008) 2360-2370.
- [7] A. Khandelwal, P. Talukdar, S. Jain, Energy savings in a building using regenerative evaporative cooling, *Energy and Buildings* 43 (2011) 581-591.
- [8] L. Giusti, M. Almoosawi, Impact of building characteristics and occupants' behavior on the electricity consumption of households in Abu Dhabi (UAE), *Energy and Buildings* 151 (2017) 534-547.
- [9] N. Ghabra, Energy Efficient Strategies for the Building Envelope of Residential Tall Buildings in Saudi Arabia, PhD Thesis University of Nottingham, UK. (2017)

- [10] D. Reiche, Energy Policies of Gulf Cooperation Council (GCC) countries—possibilities and limitations of ecological modernization in rentier states, *Energy Policy* 38 (2010) 2395-2403.
- [11] L. Z. Zhang, J. L. Niu, Performance comparisons of desiccant wheels for air dehumidification and enthalpy recovery, *Applied Thermal Engineering* 22 (2002) 1347-1367.
- [12] W.A Friess, K. Rakhshan, A review of passive envelope measures for improved building energy efficiency in the UAE, *Renewable and Sustainable Energy* 72 (2017) 485-496.
- [13] W.A. Hweij, A. A., Touma, K., Ghali, N. Ghaddar, Evaporatively-cooled window driven by solar chimney to improve energy efficiency and thermal comfort in dry desert climate, *Energy and Buildings* 139 (2017) 755-761.
- [14] K. Tsikaloudaki, T. Theodosiou, K. Laskos, D. Bikas, Assessing cooling energy performance of windows for residential buildings in the Mediterranean zone, *Energy Conversion and Management* 64 (2012) 335-343.
- [15] A. Prieto, U. Knaack, T. Klein, T. Auer, 25 Years of cooling research in office buildings: Review for the integration of cooling strategies into the building façade (1990–2014), *Renewable and Sustainable Energy* 71 (2017) 89-102.
- [16] L. Bellia, F. Francesco, M. Francesco, Effects of solar shading devices on energy requirements of standalone office buildings for Italian climates, *Applied Thermal Engineering* (2013) 190-201.
- [17] W.N. Hien, W. Liping, A.N. Chandra, A.R. Pandey, W. Xiaolin, Effects of double glazed facade on energy consumption, thermal comfort and condensation for a typical office building in Singapore, *Energy and Buildings* 37 (2005) 563-572.
- [18] A. Al Touma, K. Ghali, N. Ghaddar, N. Ismail, Solar chimney integrated with passive evaporative cooler applied on glazing surfaces, *Energy* 115 (2016) 169-179.

- [19] K. Darkwa, & P. W. O'callaghan, Simulation of phase change drywalls in a passive solar building, *Applied Thermal Engineering* 26 (2006) 853-858.
- [20] K. D. Patlitzianas, H. Doukas, J. Psarras, Enhancing renewable energy in the Arab States of the Gulf: Constraints & efforts, *Energy Policy* 34 (2006) 3719-3726.
- [21] J. R. Gosselin, Q. Chen, A dual airflow window for indoor air quality improvement and energy conservation in buildings, *HVAC&R Research* 14 (2008) 359-372.
- [22] R. Tu, X. H. Liu, Y. Jiang, Performance analysis of a two-stage desiccant cooling system, *Applied Energy* 113 (2014) 1562-1574.
- [23] P.L. Dhar, & S.K. Singh, Studies on solid desiccant-based hybrid air-conditioning systems, *Applied Thermal Engineering* 21 (2001) 119-134.
- [24] K.S. Rambhad, P. V. Walke, D. Tidke, Solid desiccant dehumidification and regeneration methods—A review, *Renewable and Sustainable Energy* 59 (2016) 73-83.
- [25] A. Afram, & F. Janabi-Sharifi, Review of modeling methods for HVAC systems, *Applied Thermal Engineering*, 67 (2014) 507-519.
- [26] M. K. Shahzad, G. Q. Chaudhary, M. Ali, N.A. Sheikh, M. S. Khalil, T. U. Rashid, Experimental evaluation of a solid desiccant system integrated with cross flow Maisotsenko cycle evaporative cooler, *Applied Thermal Engineering* 128 (2018) 1476-1487.
- [27] ASHRAE. ASHRAE handbook – HVAC systems and equipment. Atlanta, GA: American society of heating, refrigerating, and air-conditioning engineers (2008) Chapter 23.
- [28] S. Kakaç, A.E. Bergles, F. Mayinger, H. Yüncü, Heat transfer enhancement of heat exchangers, *Springer Science & Business Media* 355 (2013).
- [29] K. Ghali, M. Hourani, N.K. Ghaddar, Effective Desiccant Dehumidification System with Two-Stage Evaporative Cooling for Hot and Humid Climates 11th International Energy Conversion Engineering Conference (2013).

- [30] I. Alkhalidy, Modelling the association of dengue fever cases with temperature and relative humidity in Jeddah, Saudi Arabia—A generalized linear model with break-point analysis, *Acta Tropica* 168 (2017) 9-15.
- [31] K. Daou, R. Z. Wang, Z. Z. Xia, Desiccant cooling air conditioning: a review, *Renewable and Sustainable Energy Reviews* 10 (2006) 55-77.
- [32] P.G. Charalambous, G.G. Maidment, S.A. Kalogirou, K. Yiakoumetti, Photovoltaic thermal (PV/T) collectors: A review, *Applied Thermal Engineering* 27 (2007) 275-286.
- [33] Weather and Climate. “<https://weather-and-climate.com/average-monthly-Humidity-perc,Jeddah,Saudi-Arabia>”. 14 Jan. 2020.
- [34] S. Makarem, K. Ghali, N. Ghaddar, S. Karaki, Photovoltaic-thermal (PV/t) panel to minimize electrical and air conditioning energy consumption of a typical office in Beirut, *International Journal of Green Energy* 13 (2014) 383-394.
- [35] S. J. Slayzak, J. P. Ryan, Desiccant dehumidification wheel test guide, National Renewable Energy Lab Golden, CO (US) (2001).
- [36] M. Beccali, R. S. Adhikari, F. Butera, V. Franzitta, Update on desiccant wheel system, *International Journal of Energy Research* 28 (2004) 1043-1049.
- [37] F. Comino, M. Ruiz de Adana, & F. Peci, First and second order simplified models for the performance evaluation of low temperature activated desiccant wheels, *Energy and Buildings* 116 (2016) 574-582.
- [38] M. Mahmood, M. Sultan, T. Miyazaki, K. Shigeru, Desiccant air-conditioning system for storage of fruits and vegetables: Pakistan preview, (2016).
- [39] L. Pistocchini, S. Garone, M. Motta, Air dehumidification by cooled adsorption in silica gel grains. Part II: Theoretical analysis of the prototype testing results, *Applied Thermal Engineering* 110 (2017) 1682-1689.
- [40] A.S. Al-Ghamdi, Analysis of air-to-air rotary energy wheels, PhD diss., Ohio University, (2006)



- [41] H. Elmahdy, Thermal performance of windows, doors and shading devices: detailed calculations, *Indian Ceramics* 44 (2001) 20-24.
- [42] A. A. Zuhairy, A. Sayigh, Simulation and modeling of solar radiation in Saudi Arabia, *Renewable Energy* 6 (1995) 107–118.
- [43] AIRotor. <http://www.chetadams.com/images/2-Series>. Rotary Air-to-Air Heat and Water Vapor Exchanger. 15 Dec. 2019
- [44] ECOFRESH“DESICCANT ROTOR INTERNATIONAL.”[https://www.drirotors.com/prod\\_detail.php?prod\\_id=1](https://www.drirotors.com/prod_detail.php?prod_id=1). All Wheels Recovery Energy Some do it better. 20 Nov. 2019
- [45] D. L. Price, R. B. Simmons, I. M. Ezeonu, S. A. Crow, D. G. Ahearn, Colonization of fiberglass insulation used in heating, ventilation and air conditioning systems, *Journal of industrial microbiology* 13 (1994) 154-158.
- [46] D. G. Ahearn, S. A. Crow, R. B. Simmons, D. L. Price, J. A. Noble, S. K. Mishra, D. L. Pierson, Fungal colonization of fiberglass insulation in the air distribution system of a multi-story office building: VOC production and possible relationship to a sick building syndrome, *Journal of Industrial Microbiology* 16 (1996) 280-285.
- [47] Improve Indoor Air Quality with Fiber Glass Duct Insulation. <https://www.certainteed.com/insulation-insulation/improve-indoor-air-quality-fiber-glass-duct-insulation/>. 04. Jun. 2020
- [48] A. A. Imam, Amir, Y. A. Al-Turki, Techno-Economic Feasibility Assessment of Grid-Connected PV Systems for Residential Buildings in Saudi Arabia—A Case Study, *Sustainability* 12 (2020) 262.
- [49] H. Garg, R. Adhikari, Performance Analysis of a Combined Photovoltaic/Thermal (PV/T) Collector with Integrated CPC Troughs, 1999 ISES Solar World Congress (2000) 349–353.

- [50] B. Das, B. Rezaie, P. Jha, R. Gupta, Performance analysis of single glazed solar PVT air collector in the climatic condition of NE India, In Multidisciplinary Digital Publishing Institute Proceedings 2 (2017) 171.
- [51] A. Tiwari, M. Sodha, Parametric study of various configurations of hybrid PV/thermal air collector: Experimental validation of theoretical model, Solar Energy Materials and Solar Cells 91 (2007) 17–28.
- [52] M. Siddiqui, A. Arif, Electrical, thermal and structural performance of a cooled PV module: Transient analysis using a multiphysics model, Applied Energy 112 (2013) 300–312.4
- [53] Dai, Y. J., and K. Sumathy, Theoretical study on a cross-flow direct evaporative cooler using honeycomb paper as packing material, Applied Thermal Engineering 22 (2002) 1417-1430.
- [54] T. Itani, N. Ghaddar, & K. Ghali, Strategies for reducing energy consumption in existing office buildings, International Journal of Sustainable Energy 32 (2013) 259-275.
- [55] J. Daaboul, K. Ghali, N. Ghaddar, Mixed-mode ventilation and air conditioning as alternative for energy savings: a case study in Beirut current and future climate, Energy Efficiency 11 (2018) 13-30.
- [56] N. Ghaddar, K. Ghali, & A. Najm, Use of desiccant dehumidification to improve energy utilization in air conditioning systems in Beirut. International Journal of Energy Research 27 (2003) 1317–1338.